Ischemia/reperfusion injury : a metabolic meltdown

Wijermars, L.G.M.

V

An immediate post-reperfusion metabolic collapse associates with ischemia/reperfusion injury in the context of clinical kidney transplantation

Manuscript in preparation

Leonie G.M. Wijermars, Alexander F. Schaapherder, Dorottya K. de Vries, Lars Verschuren, Rob C.I. Wust, Sarantos Kostidis, Oleg A. Mayboroda, Amy C. Harms, Ruud Berger, Thomas Hankemeier, Jörgen Bierau, Marlies E. Reinders, Jaap F. Hamming, Jaap Bakker, Jan H.N. Lindeman

ABSTRACT

Background: kidney transplantation is the only curative option in end-stage renal disease. Due to everlasting organ shortages, more marginal grafts are used for transplantation. This leads to increased incidence of delayed graft function (DGF), the clinical readout of ischemia/reperfusion injury after transplantation. Previous studies indicated that DGF is driven by a metabolic incompetence in the (early) reperfusion period. To deepen knowledge on metabolic adaptation of DGF grafts in the acute phase of reperfusion a metabolome-broad approach was taken.
Materials & Methods: this report is based on sequential studies: a total of 52 kidney transplant recipients were included, of which 22 (16/34 and 6/18) developed DGF. Human kidney samples, taken from living donors prior to donation (n=10), served as non-ischemic controls. Renal artery and vein were cannulated during the transplantation procedure and paired plasma samples were taken immediately after reperfusion (at 0, 3, 5, 10, 20 and 30 minutes (n=34)). Biopsies were taken at the end of the ischemic period and 45 minutes after reperfusion (n=18). Metabolomics was performed on both plasma and tissue samples.
Results: DGF grafts show decreasing phosphocreatine levels (P=0,002) and ongoing ATP catabolism (i.e. persistent release of (hypo)xanthine (resp. P=0,040, P=0,007). Compared to adequately functioning control grafts, DGF grafts are hallmarked by the continuous release of lactate (P=0,001), acetylcarnitine (P=0,016), pyruvate (P=0,022), α-ketoglutarate (P=0,008), short-chain carnitines and phospholipids in the first 45 minutes after reperfusion. It was realized that the metabolomic-differences between DGF grafts and controls are collectively covered in 5 functional clusters: metabolic collapse (power outage), Krebs cycle (entry) defects, glycolysis/glutamine oxidation, lipid oxidation and phospholipolysis.
Conclusion: Incident DGF is preceded by a profound metabolic incompetence caused by mitochondrial dysfunction. Release of the Krebs cycle intermediate α-ketoglutarate, in combination with the absence of succinate recovery implies graded defects of oxoglutarate dehydrogenase activity in DGF grafts. This indicates that incident DGF not only associates with mitochondrial dysfunction, but that damage extends beyond the membrane bound respiratory complexes and also involves complexes located in the mitochondrial cytosol.

INTRODUCTION

Delayed Graft Function (DGF), clinically defined as the need for dialysis in the first week following transplantation, is the manifestation of ischemia/reperfusion injury in the context of kidney transplantation.[1,2] Incident DGF detrimentally impacts graft function and survival.[1,3] Despite major research efforts, there is currently no therapy available that prevents or alleviates clinical ischemia/reperfusion injury.[4] As such, the high incidence of DGF constitutes a major obstacle for a more liberal use of grafts donated after cardiac death and from so called marginal donors in an era of organ shortages.

In an effort to identify the factor(s) driving DGF, we systematically evaluated processes implicated in renal graft ischemia/reperfusion injury. More specifically, we sequentially assessed arterial-venous metabolite concentration differences over the reperfused renal graft to obtain organ specific information. Findings from these clinical studies challenge commonly implicated culprits of ischemia/reperfusion injury such as oxidative damage, neutrophil or complement activation, or inflammation as initiators of early ischemia/reperfusion injury.[5–9] In contrast, clear evidence was found for an association between a profound post-reperfusion metabolic deficit resulting from extensive mitochondrial damage, and incident DGF.[10]

These observations suggest that in the context of renal transplantation, ischemia/reperfusion injury is driven by a metabolic incompetence in the (early) reperfusion period. Consequently, attempts to reduce DGF should focus on preventing or overcoming the post-perfusion metabolic deficit. In this context, we considered a clinical exploration of post-reperfusion metabolic profiles of donor grafts with and without incident DGF relevant. Data from living-donor grafts; procedures with superior immediate and long-term functional outcome were included as reference profiles.

MATERIALS & METHODS

PATIENTS

The study protocol was approved by the local medical ethics committee of the Leiden University Medical Center, and written informed consent was obtained from each patient.

In this prospective study, 68 successive transplant recipients were enrolled. Ten patients refused participation, and six patients were excluded after cancellation of the transplantation (because of positive crossmatch, poor recipient condition or moderate quality of the graft). In total 52 patients were included.

Renal allograft transplantations were performed according to the local protocol.[10] In living donors, open minimal access nephrectomy was performed, and Custodiol® HTK (histidine–tryptophan–ketoglutarate) preservation solution was used for cold perfusion and storage. Deceased donor grafts were perfused and stored with University of Wisconsin solution. All included kidney transplants were preserved by means of static cold storage, none of the grafts received machine perfusion. The immunosuppressive regimen was based on induction therapy with basiliximab on day 0 and 4, and tacrolimus or cyclosporine A in addition to mycophenolate mofetil and steroids as maintenance therapy.

Patient allocation was defined by presence of delayed graft function (DGF) following transplantation. DGF was defined as the need dialysis in the first week after transplantation.[2]

ARTERIOVENOUS SAMPLING AND KIDNEY BIOPSIES

Sequential arteriovenous (AV) blood sampling over the graft was performed in 34 patients. Reference AV blood samples for a normal, non-ischemic kidney were obtained before nephrectomy by sampling over the donor kidney in living donors (n=10).

The AV sampling procedure was performed as follows: prior to implantation of the donor graft, a 5 French umbilical vein catheter was positioned in the lumen of the renal vein through one of its side branches. Renal vein blood samples were collected at 30 s, and 3, 5, 10, 20 and 30 min after reperfusion (i.e. moment of reperfusion t=0). Paired arterial blood samples (arterial line) were obtained at 0, 10 and 30 min after reperfusion. Blood samples were collected in precooled containers and immediately placed on melting ice. The AV sampling method was validated earlier measuring oxygen saturation.[7]

Renal cortical biopsies were taken immediately prior to and 45 minutes after reperfusion (n=18). Six patients received a kidney from a living donor and 12 patients received a kidney from a deceased donor. Tissue biopsies were snap frozen in liquid nitrogen and stored at –80°C.

METABOLIC ANALYSES, PLASMA

Targeted metabolomics analyses were done using standard operating procedures from previously published methods. Detailed procedures and target lists are provided in the Supplemental methods with a brief overview of the five platforms used given below.

1.Plasma amino acids

The amine platform is an UPLC-MS/MS based method that covers amino acids and biogenic amines employing an Accq-tag derivatization strategy adapted from the protocol supplied by Waters.

2.Plasma carnitines

The acylcarnitine platform is an UPLC-MS/MS based method that allows for the separation and quantification of several important isomers of acylcarnitine species as well as trimethylamine-N-oxide, choline, betaine, deoxycarnitine, and carnitine.

3.Plasma organic acids

The organic acid platform uses a full scan gas chromatography-mass spectrometry (GC-MS) method combined with a target list of well-characterized metabolites for the analysis of organic acids. The method uses a combination of an oximation reaction using methoxyamine hydrochloride and a silylation reaction using N-Methyl-N-(trimethylsilyl) trifluoroacetamide.

4.Plasma purines and pyrimidines

Purines and pyrimidines were quantified using an in-house developed UPLC-MS/MS method using a Waters Acquity HSS T3 column and a Waters XEVO TQS tandem mass spectrometer using negative or positive electrospray ionization with specific MRM transitions.

METABOLIC ANALYSES: TISSUE (KIDNEY BIOPSIES)

5.Magic Angle Spinning High-resolution NMR spectroscopy (MAS HR-NMR)

Metabolic profiling of the tissue biopsies was performed by MAS HR-NMR spectrometry on a 14.1 T Bruker Avance III spectrometer. All measurements were performed at the MR Core Facility, Norwegian University of Science and Technology (NTNU). The MR core facility is funded by the Faculty of Medicine at NTNU and Central Norway Regional Health Authority.

STATISTICAL ANALYSIS

SPSS 22.0 (SPSSinc, Chicago, III) was used for statistical analysis. For heatmaps of arteriovenous concentrations differences between the three groups, venous/arterial ratios were calculated and expressed as the mean Z-score for each metabolite. For the heatmaps of tissue levels, pre-reperfusion/post-reperfusion rates were calculated and expressed in mean Z-score of the quantified concentrations. AV differences (per timepoint) were compared by Students T-test within group and tested with ANOVA between groups. Pre- and post-reperfusion levels of tissue metabolites were compared by Students T-test within group and pre/post reperfusion rates were compared and tested with ANOVA between groups.

If indicated, the area under the curve (AUC) was estimated for some plasma metabolites and compared through a linear mixed model analysis for arterial and venous measurements for the total of 30 min. The model contained as independent variables time, as categorical the group (Living vs. –DGF vs. +DGF), and the interaction between group and time. The covariance model was specified as unstructured. The delta AUC was calculated (venous minus arterial) and the null hypothesis (AUC=0) was tested by a Wald test based on the estimated parameters of the linear mixed model.

Since most metabolites in the study are part of theoretical pathways we refrained from correction for multiple testing.

RESULTS

This study is based on data from a total of 52 kidney transplantations, 38 of these procedures concerned deceased donor graft transplant procedures. The clinical follow up showed that 22 of the deceased donor grafts fulfilled the criteria for DGF. These grafts were allocated to the +DGF group. The other 16 deceased donor grafts all displayed spontaneous recovery without the need for post-transplant dialysis and were therefore allocated to the –DGF group. Fourteen procedures concerned living donor grafts. All living grafts showed immediate functional recovery following reperfusion (urine production and creatinine clearance) and served as a reference. All grafts in the study showed ultimate functional recovery. Clinical details for the different groups are shown in Table 1).

Table 1. Patient characteristics

Patient Characteristics for arteriovenous concentration differences			
	Living (n=8)	Deceased – DGF (n=10)	Deceased +DGF (n=16)
Age recipient (yrs)	58,5±5,0	49,0±12,6	59,1±11,9
Sex recipient (% males)	55,6%	50%	68,8%
Recipient – cause of renal failure			
Glomerulonefritis	44,4%	40,0%	31,3%
*Polycystic kidney disease	11,1%	20,0%	18,8%
*DM type 2	0%	0%	25,0%
*Obstructive uropathy	11,1%	10,0%	6,25%
*Maligne hypertension	11,1%	20,0%	12,5%
*Renal failure e.c.i.	22,2%	10,0%	6,25%
Age donor (yrs)	55,5±10,7	55,6±13,8	57,4±15,3
Sex donor (% males)	66,7%	60%	56,2%
Donor cause of death			
*Living donor	100%	0%	0,0%
*CVA		20,0%	25,0%
*SAB		30,0%	12,5%
*TRAUMA		30,0%	25,0%
*CA-OHCA-AMI		20,0%	31,3%
*Suicide		0%	6,25%
*Miscellaneous		0%	0,0%
Ischemia time (hrs)	3,6±0,4	18,2±4,4	17,9±5,7
Histocompatibility (HLA mismatches, %)			

0	0%	10,0%	0,0%
1	33,3%	0%	18,8%
2	0%	60,0%	18,8%
3	11,1%	20,0%	37,5%
4	11,1%	10,0%	12,5%
5	33,3%	0%	12,5%
6	11,1%	0%	0,0%
Hospital Stay (days)	7,14±3,5	10,2±4,9	19,8±7,8

Patient Characteristics for HR MAS NMR spectroscopy in kidney biopsies			
	Living (n= 6)	Deceased – DGF (n= 6)	Deceased +DGF (n= 6)
Age recipient (yrs)	48,5±18.0	52,8±16,9	59,8±11,5
Sex recipient (% males)	100%	50%	100%
Recipient – cause of renal failure			
Glomerulonefritis	16,7%	33,3%	0%
*Polycystic kidney disease	16,7%	16,7%	16,7%
*DM type 2	16,7%	33,3%	33,3%
*Obstructive uropathy	16,7%	0%	0%
*Maligne hypertension	16,7%	16,7%	0%
*Renal failure e.c.i.	16,7%	0%	50%
Age donor (yrs)	50±8.1	59,3±11,3	56,5±13,2
Sex donor (% males)	66,7%	50%	33,3%
Donor cause of death			
*Living donor	100%	0%	0%
*CVA		33,3%	33,3%
*SAB		33,3%	0%
*TRAUMA		0%	16,7%
*CA-OHCA-AMI		33,3%	50%
*Suicide		0%	0%
*Miscellaneous		0%	0%
Ischemia time (hrs)	3,7±0,3	10,4±2,9	16,5±3,9
Histocompatibility (HLA mismatches, %)			
0	0%	0%	0%
1	0%	16,7%	0%
2	16,7%	16,7%	16,7%
3	16,7%	16,7%	50%
4	16,7%	33,3%	16,7%
5	33,3%	16,7%	16,7%
6	16,7%	0%	0%
Hospital Stay (days)	6,7±1,2	9,4±4,6	18,0±8,9

Table 1. Patient Characteristics. Patients were included in two recruitery rounds. Recipients of living donor grafts were taken as a reference since DGF is rare in this control group. Deceased donor grafts were classified based on outcome after transplantation. Delayed graft function (DGF) is status in which the transplant recipient is in need of dialysis in the first week(s) after transplantation and is caused by I/R injury.
Abbreviations: DM = diabetes mellitus, e.c.i. = e causa ignota.

We first explored putative differences in the metabolic signatures of +DGF deceased donor grafts, –DGF deceased donor grafts and those of the living donor grafts (reference) of the T=30 min post-reperfusion AV differences and the post-reperfusion tissue biopsies. The 30 min time-point for the AV differences was chosen to avoid interference from washout of metabolites accumulated during ischemia.
The AV differences are summarized in the heatmap shown in Figure 1A, and the tissue profiles in Figure 1B. The heatmap for the AV differences (Fig. 1A) shows parallel signatures for the living donor grafts and –DGF grafts, and a distinctive signature for the +DGF grafts. Although, differences on the tissue level (Figure 1B) were less outspoken than those for the AV differences, the –DGF signature matched that of the living donor reference group.
Functional clustering of the individual metabolic differences between –DGF and +DGF grafts identified 5 functional clusters: (I) metabolic collapse (power outage); (II) beta-oxidation; (III) glycolysis/glutamine oxidation and autophagy; (IV) Krebs cycle (entry) defects, and (V) phospholipolysis/cell damage. Collectively, these clusters cover all observed metabolic differences (the metabolic signature of future DGF). For the sake of clarity, it was decided to report the metabolites according to this clustering.

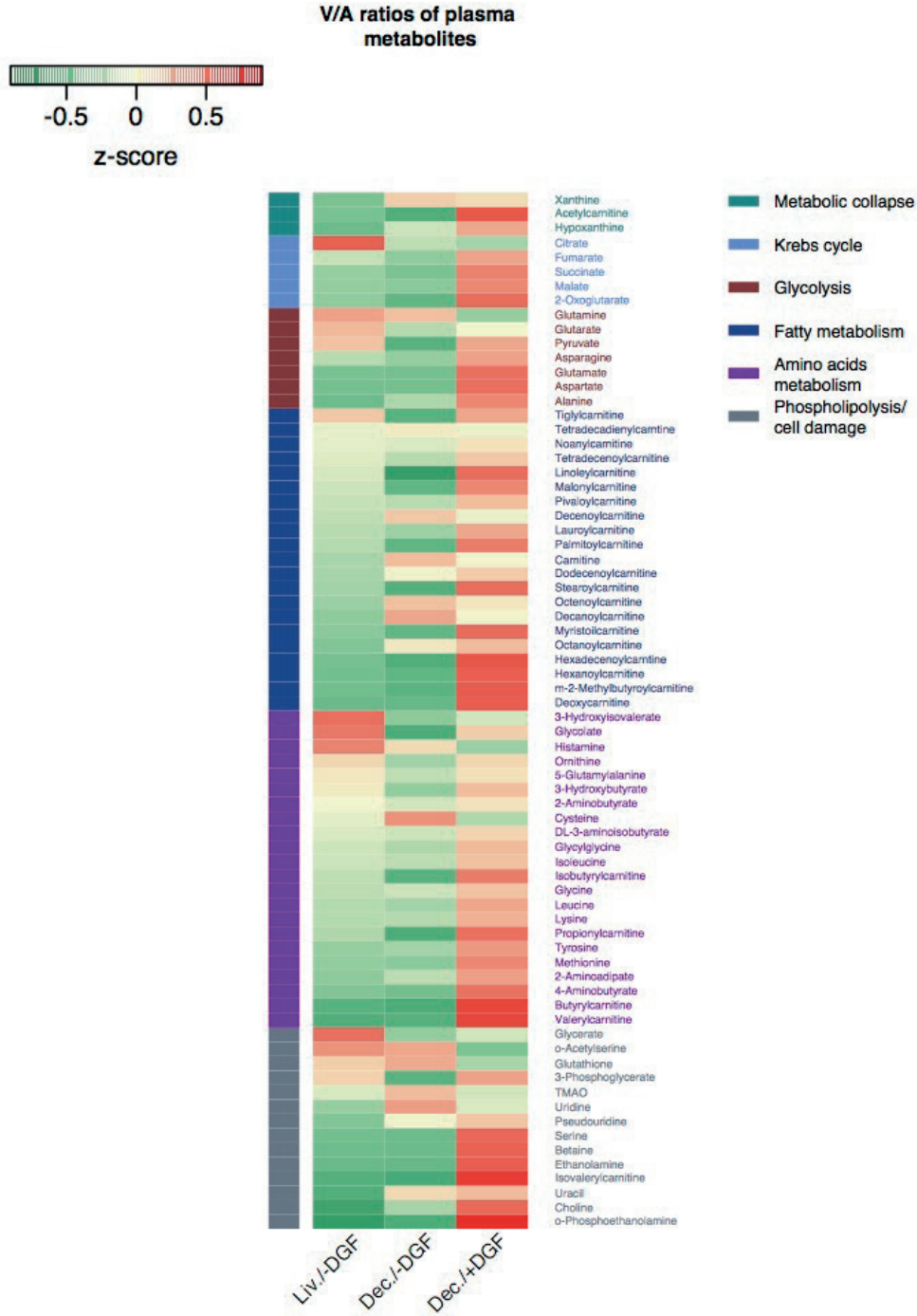

Figure 1A. Clustered heatmap for the arterial-venous metabolite concentration differences over the donor graft at 30 minutes after reperfusion.

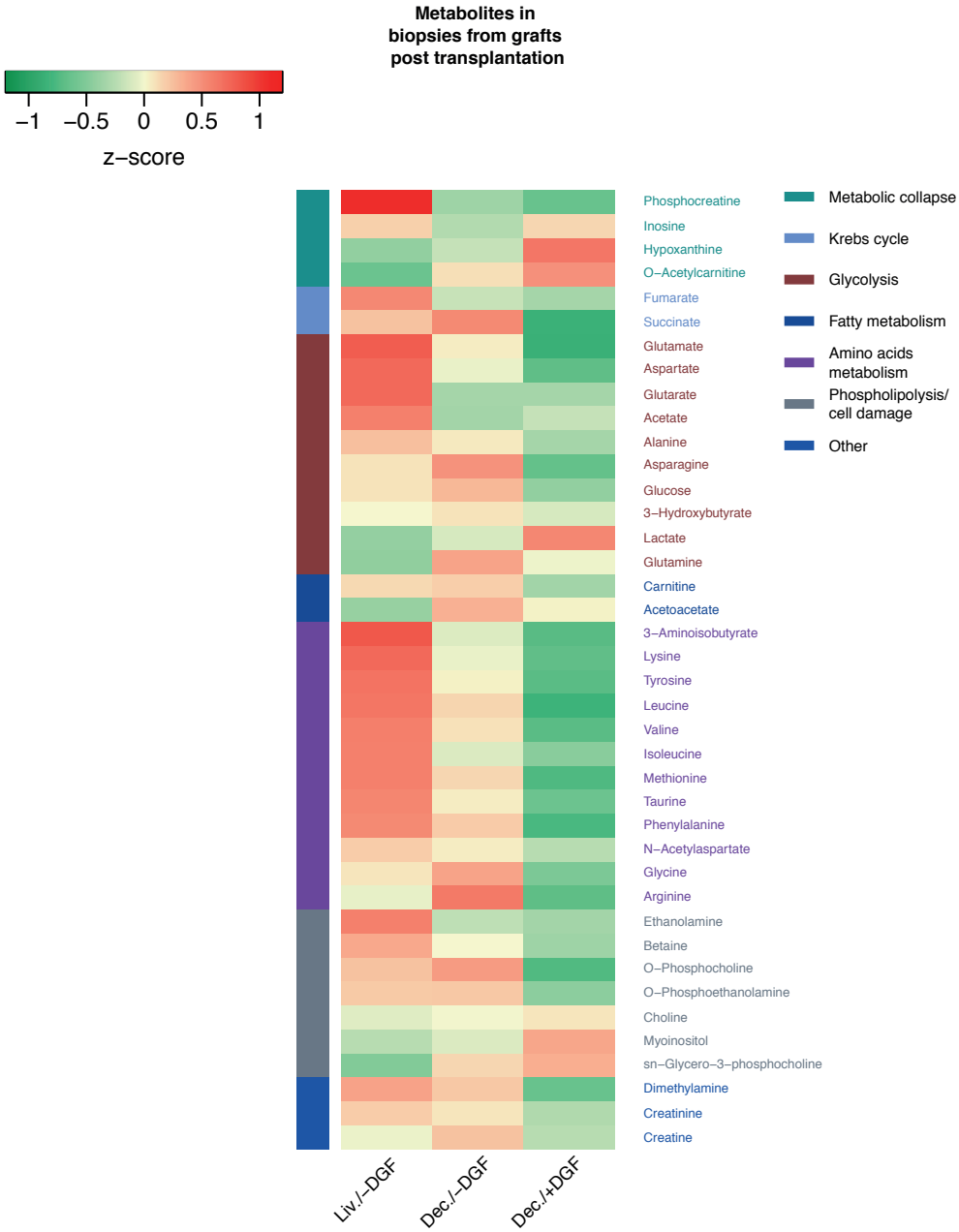

Figure 1B. Clustered heatmap for all identified tissue metabolites in the HR magic angle NMR analysis of graft biopsies taken 40 minutes after reperfusion.

Figure 1A. Clustered heatmap for the arterial-venous metabolite concentration differences over the donor graft at 30 minutes after reperfusion.
The three columns represent the three donor groups (living donor grafts (reference group); deceased donor grafts without later DGF (–DGF), and deceased donor grafts with later DGF (+DGF). Rows represent the arteriovenous concentrations differences between the three groups, expressed as the mean Z-score of the venous/ arterial ratios for each metabolite. Compounds are clustered according to the five metabolic clusters and, within each cluster ranked on basis of the Z-score of the living donors group. Green reflects net uptake by-, and red net release from the graft.

Figure 1B. Clustered heatmap for all identified tissue metabolites in the HR magic angle NMR analysis of graft biopsies taken 40 minutes after reperfusion. The three columns represent the three donor groups (living donor group (reference group), deceased donor grafts without later DGF (–DGF) and deceased donor grafts with later DGF (+DGF). Rows represent tissue content of each metabolite, expressed in mean Z-score of the quantified concentrations. Metabolites are clustered according to the five metabolic clusters and, within each cluster, ranked on basis of the Z-score in the living donor group. Red reflects a tissue content above, and green below the geometric mean of the three groups.

The first cluster of metabolites is consistent with a metabolic collapse ('power outage') in grafts with later DGF. This collapse is reflected by absent recovery of the high-energy phosphate buffer phosphocreatine in the tissue of +DGF grafts ($P<0.002$, Figure 2A), and by persistent hypoxanthine and xanthine release (AV-differences) from these grafts (Figure 2B). Although all 3 graft types showed an initial wash out of these ATP/GTP catabolites upon reperfusion, persistent release in grafts with later DGF implies continued ATP/GTP catabolism after reperfusion ($P<0.007$ and $P<0.04$ respectively for hypoxanthine and xanthine at T=30 min). Graded pre-reperfusion tissue accumulation of the ATP catabolites inosine and hypoxanthine in the three donor groups with the lowest tissue content in living, and the highest in +DGF donor grafts (Figure 2C) implies progressive degrees of high energy phosphate depletion during organ procurement and cold preservation. Low post-reperfusion contents in the +DGF group presumably relate to circulatory clearance (hypoxanthine), but possibly also to exhaustion of the ATP supply in these grafts.

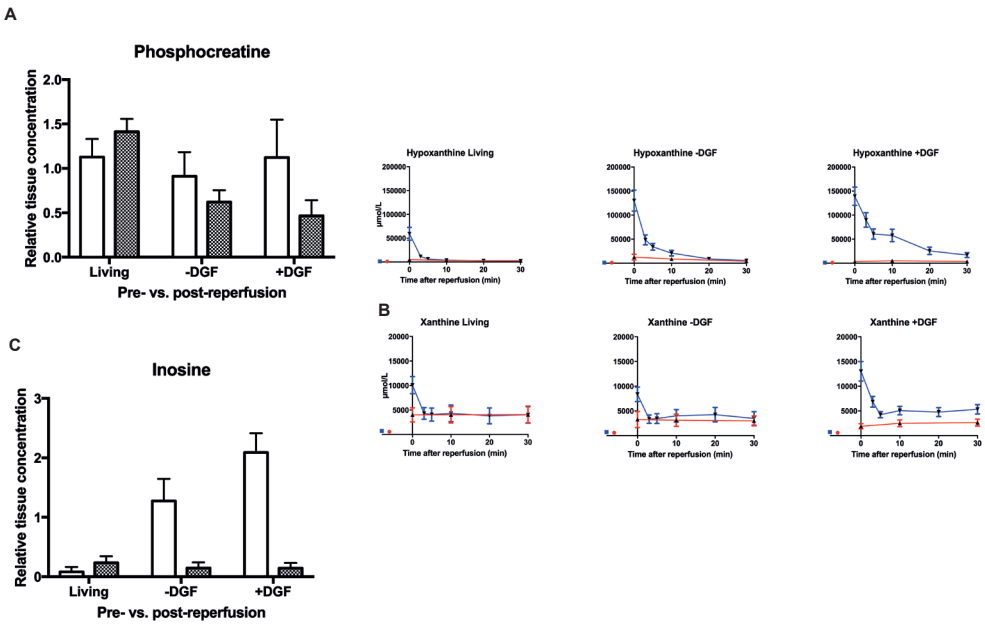

Figure 2. A post-reperfusion metabolic collapse associates with future DGF.
A) Pre and post-reperfusion(40 minutes post reperfusion) tissue phosphocreatine content in the three donor groups (living donor group (reference group), deceased donor grafts without later DGF (–DGF) and deceased donor grafts with later DGF (+DGF)). Stable post-reperfusion tissue phosphocreatine content in living donor grafts and –DGF grafts , but reduced post-reperfusion phosphocreatine tissue content (P‹0.002) in grafts with later DGF.
B) Post-reperfusion arterial (red) and venous (blue) concentrations for hypoxanthine and xanthine, the end products of nucleoside triphosphate catabolism. Stable arterial hypoxanthine and xanthine levels in all three study groups. Renal vein samples show an immediate wash out of accumulated hypoxanthine and xanthine following reperfusion in all three study groups. Persistent hypoxanthine and xanthine release from +DGF grafts (P‹0.007 and 0.04 respectively at T= 30 minutes after reperfusion) implies persistent nucleoside triphosphate catabolism in these grafts.
C) Progressive pre-reperfusion accumulation of inosine in the three graft types showing implying graded ATP catabolism during organ procurement.

Arterial (red) and venous (blue) data points left at the curve indicate plasma levels over normal kidneys.

The metabolic deficit in +DGF grafts occurred in spite of restoration of β-oxidation (Figure 3) and activation of normoxic glycolysis (Figure 4) and possibly autophagy (Figure 5). Uniform restoration of β-oxidation in all 3 graft types is reflected by emergence of hydroxybutyric acid in post-reperfusion tissue biopsies, as well as by clearance (uptake) of mid-chain fatty acids (C8-C12) from the circulation (Figure 3; Supplemental Figures). Tissue accumulation (-DGF and +DGF grafts) (Fig. 3C) and release of acetyl-carnitine in the circulation (Fig.3B) (+DGF grafts) (T=30 min: P‹0.016) implies various degrees of impaired disposal of this end-product of β-oxidation in the deceased donor grafts.

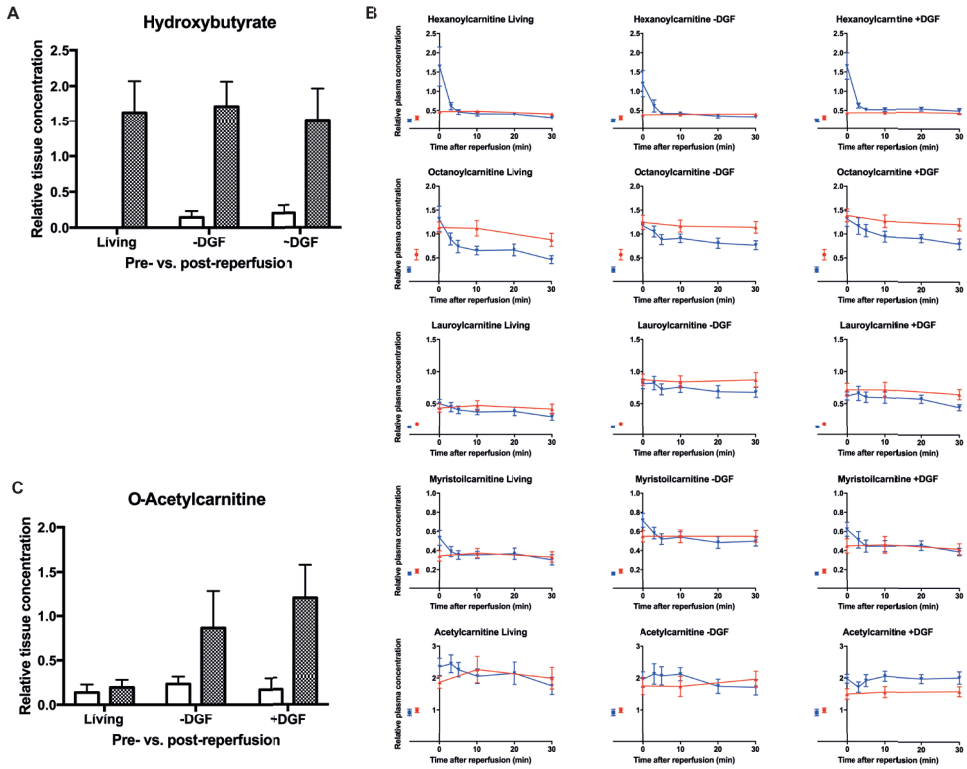

Figure 3. Reinstatement of β-oxidation (medium chain fatty acids) following reperfusion.

A) Post-reperfusion recovery hydroxybutyrate showing commencement of β-oxidation in all three donor groups

B) A-V differences for plasma carnitines show selective uptake of C8-C12 medium chain carnitines in all three donor groups. Transient (-DGF) and persistent acetylcarnitine release (AV differences, P‹0.007) and acetylcarnitine tissue accumulation C) indicate temporary respectively persistent inadequate acetyl disposal in – and +DGF grafts.

Arterial (red) and venous (blue) data points left at the curve indicate plasma levels over normal kidneys.

Mapping of glycolysis/glutaminolysis (Figure 4) indicated absent recovery of tissue glucose content following reperfusion, and persistent glycolysis in the +DGF donor grafts. Normoxic glycolysis in +DGF grafts is illustrated by the persistent release of lactate (T=30 min: $P<0.001$) and the transamination products alanine and aspartate (T=30 min: $P<0.006$ and $P<0.005$ respectively, Figure 4). Evident glutamine uptake and glutamic acid release (T=30 min: $P<0.006$) (AV differences) by the +DGF grafts points to a contribution of glutaminolysis in the energy supply. +DGF grafts showed net pyruvate release in the reperfusion phase (T=30 min: $P<0.022$), indicating that pyruvate production in these grafts exceeds pyruvate disposal (LDH, transaminases, Krebs cycle). Note that stable tissue glutamine, glutamate, alanine, and aspartate levels in +DGF grafts suggest an efficient blood-tissue exchange of these metabolites.

Some indications were found for autophagy (Figure 5) in +DGF grafts such as the net-release (AV differences) of selective amino-acids such as methionine and tyrosine (P for the area under the curves of methionine release in To-30 min after reperfusion: $P<0,000006$ and $P<2,3993E^{-7}$ respectively)) Figure 5). In this respect, progressive isovaleryl-carnitine release in +DGF indicates post-reperfusion leucine oxidation in these grafts.

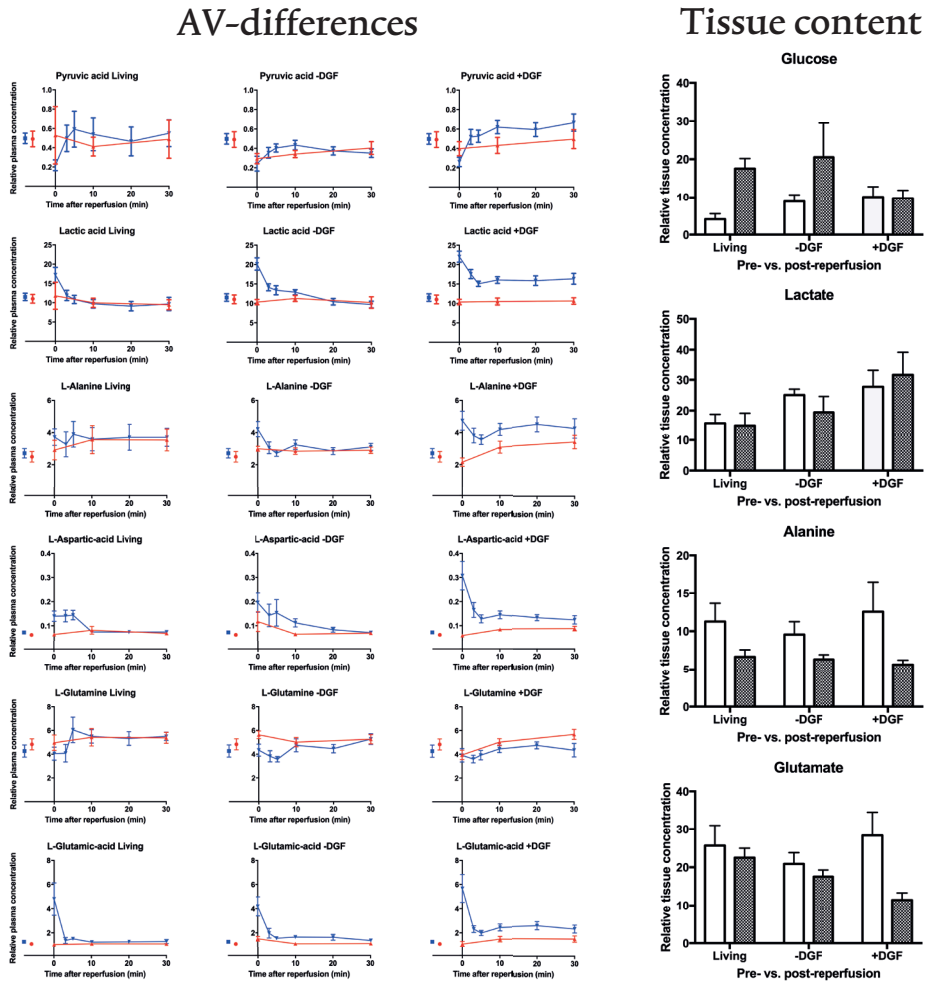

Figure 4. Post-reperfusion glycolysis and glutaminolysis.
Left column: A-V differences. Persistent post-reperfusion lactate, alanine (P‹0,006) and pyruvate (0.022) release from +DGF grafts indicate normoxic glycolysis in these grafts. Temporary resp. continued glutamine uptake and glutamate release (P‹0.006, (AV differences) from – and + DGF grafts show transient and persistent glutamine oxidation in these grafts.
Right column: tissue content. Pre and post reperfusion tissue contents of glucose, lactate, alanine and glutamine. Absent glucose recovery and persistently high lactate content in +DGF grafts. Stable alanine and glutamate contents presumably reflect wash out of these intermediates from the kidney.
Arterial (red) and venous (blue) data points left at the curve indicate plasma levels over normal kidneys.

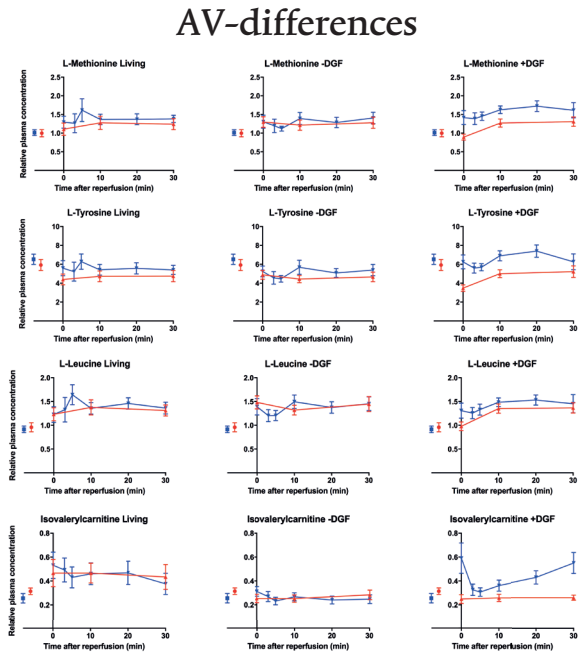

Figure 5. Post reperfusion amino acid metabolism.
A-V differences show post-reperfusion net release of the methionine, and the ketogenic amino acids tyrosine and leucine (P=0,000006; P=2,3993E-7 and P=0,017) from + DGF grafts. Selective and progressive isovalerylcarnitine release indicates post-reperfusion leucine oxidation in +DGF grafts.
Arterial (red) and venous (blue) data points left at the curve indicate plasma levels over normal kidneys.

The apparent metabolic deficit despite abundant activation of beta-oxidation, glycolysis and possibly autophagy, and the accumulation of the Krebs cycle entry-products acetyl-carnitine (Figure 3) and pyruvate (Figure 4) point to Krebs cycle defect(s) (Figure 6, Supplemental Figure 1) in +DGF grafts. Post-reperfusion release of the Krebs cycle intermediate α-ketoglutarate (T=30 min: P<0.008, Figure 6), but not its downstream intermediates succinate, fumarate and malate, and absent recovery of tissue succinate and fumarate in the +DGF grafts (Figure 6) indicate at least a defect at the level of oxoglutarate dehydrogenase in +DGF grafts.

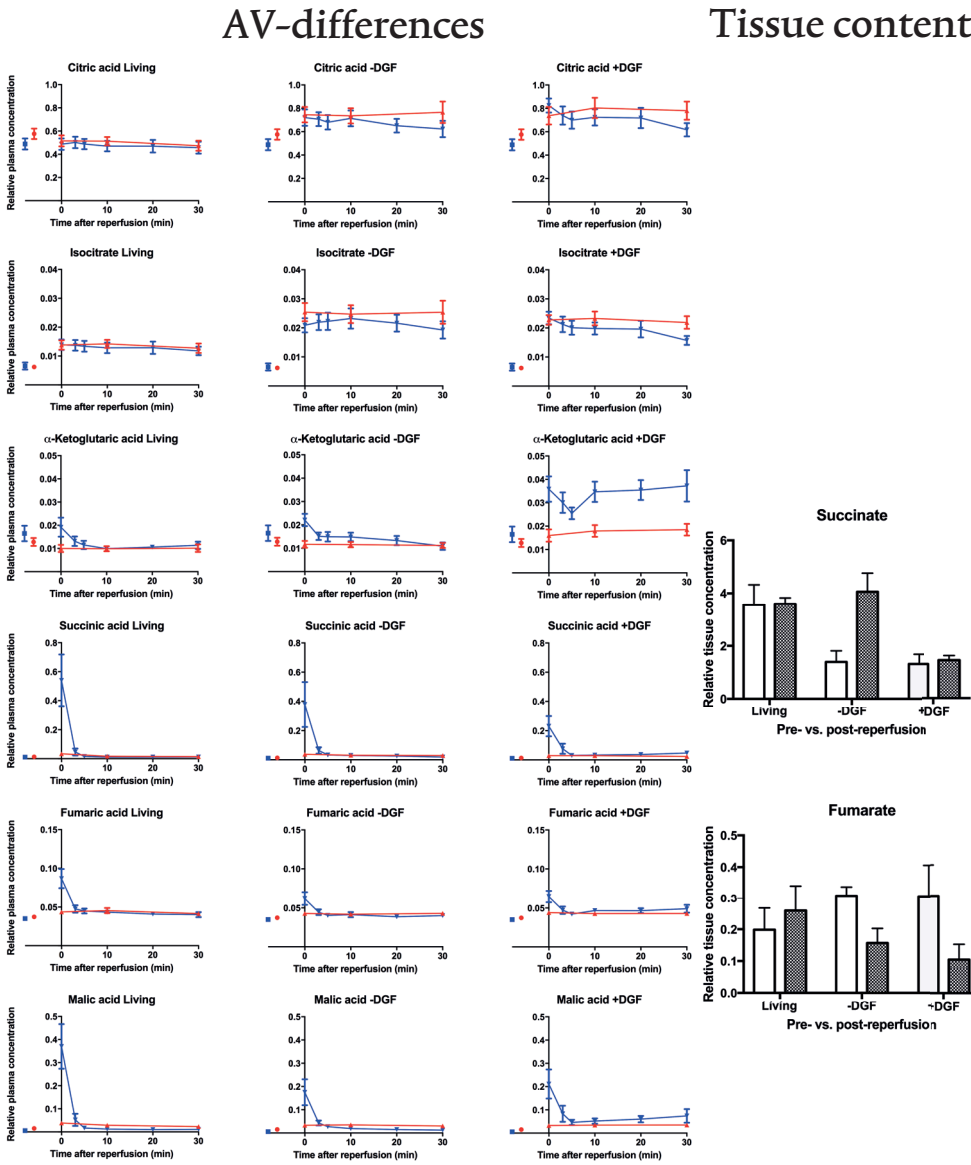

Figure 6. Post-reperfusion Krebs cycle defect in grafts with future DGF.
Left column: A-V differences. Release of the Krebs cycle intermediate α-ketoglutarate from +DGF grafts
Right column: tissue content. Absent succinate (+DGF grafts) and fumarate (- and +DGF grafts) recovery.
Arterial (red) and venous (blue) data points left at the curve indicate plasma levels over normal kidneys.

Results from the amino acid and purine analysis revealed a further discriminatory pattern that is consistent with post-reperfusion phospholipolysis/cell damage in +DGF grafts (Figure 7). This pattern includes release of uracil (T=30 min: P‹0.0002) and release of a cluster of phospholipid associated amino-acid constituents (viz. phospho-ethanolamine, ethanolamine, and phospho-serine (P for T=30 min resp.: ‹0.001, ‹0.004 and ‹0.003). Although choline was not released, its oxidation product betaine was progressively and selectively released from +DGF grafts (T=30 min: P‹0.0004).
Again, stable tissue content for these markers implies efficient tissue clearance and/or metabolism.

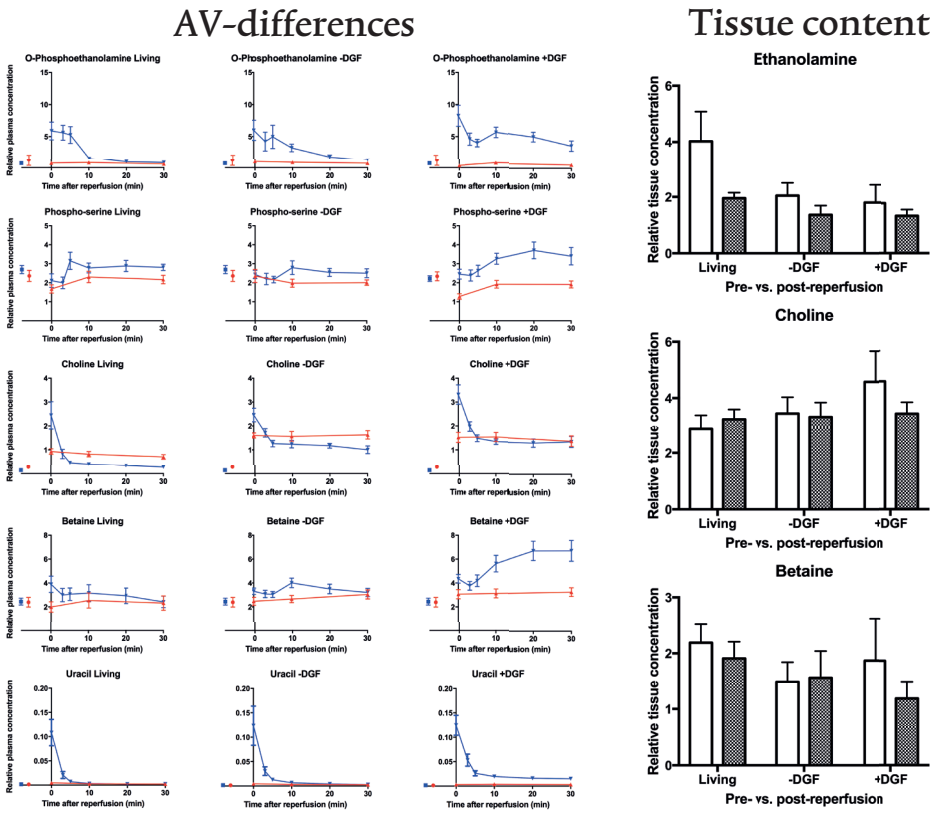

Figure 7. Selective and persistent post-reperfusion wash out of phospholipid-associated amino-acids and uracil from grafts with future DGF.
Initial and brief wash out of accumulated the phospholipid components (phospho) ethanolamine, and choline, and the pyrimidine uracil upon reperfusion for all three donor groups. A-V differences show persistent release of uracil (T=30 min: P‹0.00002), and phospholipid-associated amino acids (phosphor) ethanolamine, phosphoserine. Progressive post-reperfusion release of betaine, (T=30 min: P‹0.0004) the oxidation product of choline from +DGF grafts implies post-reperfusion choline oxidation. Tissue ethanolamine and betaine remain stable.
Arterial (red) and venous (blue) data points left at the curve indicate plasma levels over normal kidneys.

Above observations associate the incident ischemia/reperfusion injury with persistent post-reperfusion ATP catabolism and on-going cell damage in a context of mitochondrial failure and activation of glycolytic and lipolytic pathways.

DISCUSSION

From this study, performed during clinical kidney transplantation, the picture emerges of human renal ischemia/reperfusion injury being the consequence of an instantaneous, profound metabolic collapse in the early reperfusion phase. As a consequence, cells are unable to sustain adequate ATP levels, critically impairing their integrity, and perpetuating cellular injury. The data herein imply fundamentally different mechanisms for ischemia/reperfusion injury in humans compared to rodents.[11]

Conclusions from this study are based on integration of tissue data derived from paired pre- and post-reperfusion tissue biopsies and plasma-derived data based on sequential arteriovenous concentration differences over de graft during the first half hour of reperfusion. The plasma data allow for the appreciation of metabolite clearance into (elimination) or from (uptake) the circulation[12] and for directing the data from the paired tissue biopsies. In fact, we realized that sole reliance on tissue biopsies would have obscured most occurring events, as metabolite tissue levels/content remained stable due to effective clearance into the blood. Note that deceased donor grafts are anuric in the time frame of this study. As such, observations for the deceased donor grafts are not influenced by urinary metabolite clearance.
Mapping of the available metabolic data, shows that incident DGF (as a result of excessive tissue damage) is preceded by a metabolic crisis with persistent ATP catabolism in the reperfusion phase. This crisis is fully discriminatory for +DGF grafts, and appears to be primarily related to defects in the normoxic respiration (Krebs cycle defects), and an activated normoxic glycolysis that is unable to sustain the ATP supply. This latter conclusion is based on absent tissue phosphocreatine recovery,[13] and persistent post-reperfusion hypoxanthine and xanthine release in +DGF grafts. Hypoxanthine and xanthine represent end products of ATP (hypoxanthine and xanthine) and GTP (xanthine) degradation. Consequently, their continued release from +DGF grafts implies persistent ATP/GTP catabolism despite adequate graft perfusion (viz. oxygen and glucose supply). In fact, on basis of the reported post reperfusion renal blood flow it is estimated that the hypoxanthine lost in +DGF grafts during the first half hour of reperfusion represents more than 50% of the renal ATP pool/storage.

Impaired ATP regeneration in +DGF grafts appears to (partly) relate to impaired oxidative phosphorylation as result of Krebs cycle defect(s). This conclusion is based on release of pyruvate, and particular acetyl-carnitine, which indicates that these carbon flows exceed the capacity of the Krebs cycle; the release of the Krebs

cycle intermediate α-ketoglutarate, and absent tissue succinate recovery. Although it cannot be excluded that the α-ketoglutarate excess partly relates to glutamine oxidation, absent tissue succinate recovery in +DGF grafts, and to a lesser extend in –DGF grafts implies graded defects of oxoglutarate dehydrogenase activity.
These data extend conclusions from experimental studies and our earlier report that incident DGF associates with mitochondrial dysfunction[10,14] and that this damage not only extends beyond the membrane bound respiratory complexes, but also involves complexes located in the mitochondrial cytosol. Fully preserved β-oxidation in +DGF grafts shows that these effects are specific, and do not merely reflect gross mitochondrial damage.
An apparent persistent defect at the level of oxoglutarate dehydrogenase and absent succinate accumulation point to fundamental differences in the mechanisms involved in human and rodent (renal) ischemia and reperfusion. In fact, reported data for rat kidneys (and other organs) imply an oxidative burst within the first minutes of reperfusion, which is then followed by normalization of oxidative phosphorylation.[11] Human data herein imply a more protracted process with persistent mitochondrial failure, high-energy phosphate deficiencies, and absent gross oxidative damage.

Defects in oxidative phosphorylation in +DGF grafts are partially compensated by recruitment of normoxic glycolysis, as reflected by the continued lactate, alanine and asparagine release from these grafts, and possibly by the low post-reperfusion tissue glucose content. Although the latter could obviously relate to the increased glycolysis it cannot be excluded that a context of (relative) ATP deficiency interferes with insulin-mediated glucose uptake. Release of pyruvate in the circulation indicates that pyruvate flux in +DGF grafts exceeds the capacity of pyruvate dehydrogenase, lactate dehydrogenase, and aspartate transaminase and alanine transaminase.
Normoxic glycolysis in the +DGF grafts was paralleled by persistent glutaminolysis as shown by the glutamine uptake and glutamate release into the circulation. Early reperfusion glutamine uptake seen in living donor and –DGF grafts suggests transient glutamine oxidation as a metabolic adaptation in the first minutes following reperfusion.

The 3 graft groups showed similar post-reperfusion recruitment of lipid oxidation with recovery of tissue hydroxybutyrate and uptake of medium chain carnitines (C8-C12) and unsaturated C14 from the circulation. This latter observation implies that the kinetics of unsaturated C14 corresponds to that of a medium chain fatty acid. There appears to be a small but consistent release of short chain (C6 and smaller) carnitines from +DGF grafts. This phenomenon may indicate peroxisomal

β-oxidation since this reaction is limited to large and medium chain lipids and absent for smaller acyl chains. As peroxisomal lipid oxidations lack a valid electron acceptor, it is paralleled by a stoichiometric production of hydrogen peroxide. Consequently, putative peroxisomal β-oxidation in +DGF grafts merits attention as a route that may perpetuate ischemia/reperfusion injury through production of hydrogen peroxide.

The data for the amino acids identified 3 functional clusters. A cluster that relates to the process of glycolysis/glutaminolysis discussed earlier, a second cluster that is particularly enriched for amino acids incorporated in glycerophospholipids (see further), and a third cluster (methionine, tyrosine, serine and isovalerylcarnitine) that presumable reflects autophagy and failure to (completely) metabolize amino acids. The notion of autophagy and incomplete amino acid catabolism is supported by the isovalerylcarnitine release from +DGF grafts. Isovaleryl-CoA is an intermediate of leucine catabolism, that is normally further oxidized by isovaleryl-CoA dehydrogenase. In this context, selective release of isovalerylcarnitine may reflect excess substrate delivery (leucine from autophagy) and/or ischemia/reperfusion-related defects in the isovaleryl-CoA dehydrogenase complex.
We have no clear explanation for the asymmetrical amino acid release pattern (viz. release of abundant amino acids such as leucine and serine, but not of glycine). One possibility is that acetyl-CoA or NADPH accumulation in +DGF grafts interferes with leucine and serine catabolism. Albeit interesting and potentially relevant, we consider further exploration of observed asymmetrical amino acid release beyond the scope of this explorative paper.
Selective and sustained release of a class of amino acids is almost exclusively associated with glycerophospholipids in +DGF grafts, and implies that incident renal ischemia/reperfusion injury is associated with immediate cell membrane damage following reperfusion. In this context, the data for betaine, the oxidation product of choline is particularly revealing. While pre- and post-reperfusion tissue betaine levels remain stable, there is a selective and delayed post-reperfusion release of betaine from +DGF grafts. This observation implies post-reperfusion choline availability in +DGF grafts and that release of glycerophosolipid-associated amino acids is a reperfusion-related phenomenon, rather than a phenomenon related to ischemia-related damage. The pattern of sustained damage (phospholipolysis, uracil release) in +DGF grafts suggests clinical reperfusion injury is a protracted event. This notion is supported by release patterns of the Krebs cycle intermediates.

All in all, above conclusions imply that the mitochondrial defects and the associated metabolic collapse occur within the first minute(s) of reperfusion,

leaving a marginal window of opportunity for rescue therapies aimed at mitochondrial stabilization. Yet, unlike other forms of ischemia and reperfusion, organ transplantation does allow for preventive strategies aimed at mitochondrial stabilization. As such, in the context of organ transplantation (and other forms of planned ischemia and reperfusion), strategies aimed at mitochondrial stabilization, either as donor treatment or during organ storage (preservation) merit attention.[15,16]

Alternative, non-preventative strategies should focus on maximizing the available energy resources, in particular for normoxic glycolysis. Such an approach could include optimal substrate delivery and/or inhibition of futile or inhibitory pathways. In-depth analysis of the erythrocyte, a professional aerobic glycolytic cell that is devoid of mitochondria identified inosine as an energy dense alternative for glucose. Along this lines, inosine is superior to glucose in preserved cellular ATP content of eukaryotic cells during hypoxia[17] and ameliorates tissue damage in experimental ischemia/reperfusion models.[18,19]

Strategies improving aerobic glycolysis could further include reduction of cellular acidosis via minimizing H+ formation in futile metabolic cycles. Reflexive pyruvate formation via activation of glutaminolysis is the natural response of somatic cells aimed at sustaining the Krebs cycle. Observed pyruvate release, and α-ketoglutarate from +DGF grafts show that, in the context of graft ischemia/reperfusion injury glutaminolysis is futile, yet does potentially contribute to cellular acidosis via release of H+ and consumption of NAD+. One could speculate that in such a context interference with glutaminolysis is beneficial.

In conclusion, results of this clinical evaluation show that incident graft ischemia/reperfusion injury is preceded by a profound metabolic incompetence caused by mitochondrial dysfunction, shedding light on the underlying mechanism of clinical ischemia/reperfusion injury. It came to our attention that although this difference may relate to fundamental differences in the pathophysiology of ischemia and reperfusion between rodent and humans, it may also imply that the injury inflicted in rodent models is insufficient to induce the metabolic deficit observed in human renal ischemia/reperfusion injury.

SUPPLEMENTARY FIGURES

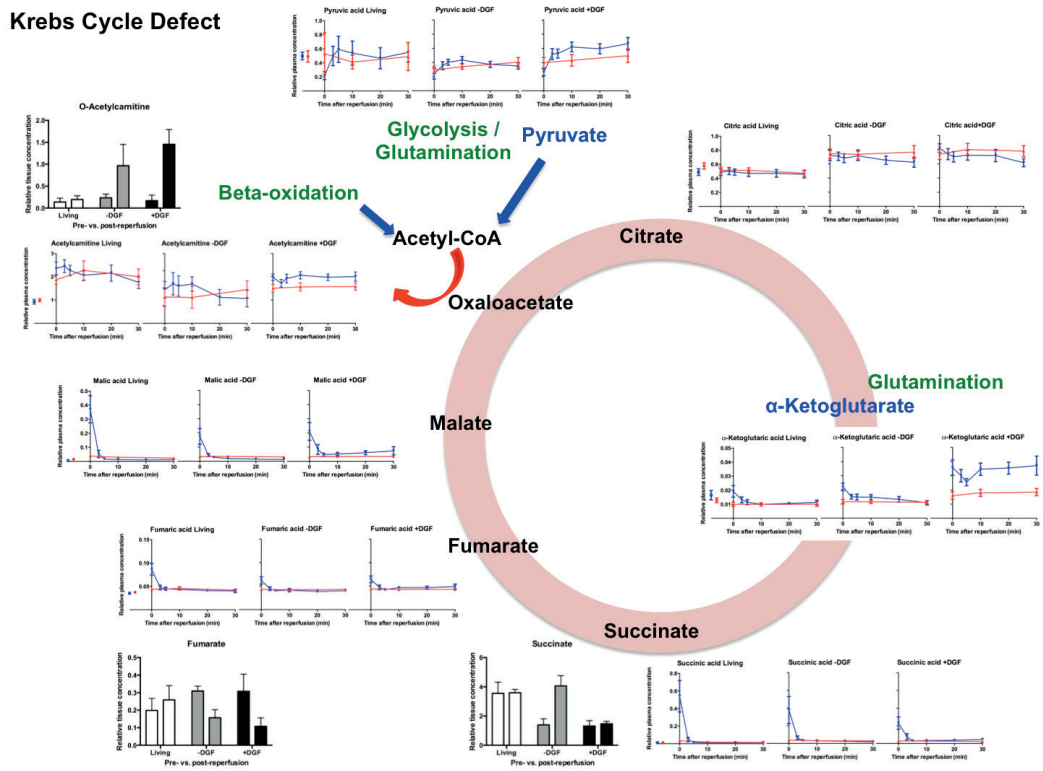

Supplemental Figure 1. Krebs Cycle (entry) Defect.
Accumulation of the Krebs cycle entry-products O-acetylcarnitine (P‹0,004), release of acetylcarnitine (T=30; P‹0,016), and pyruvate point to Krebs cycle defect(s) in +DGF grafts. Post-reperfusion release of the Krebs cycle intermediate α-ketoglutarate (T=30 min: P‹0.008), but not its downstream intermediates succinate, fumarate and malate, and absent recovery of tissue succinate and fumarate in the +DGF grafts indicate at least a defect at the level of oxoglutarate dehydrogenase in +DGF grafts.

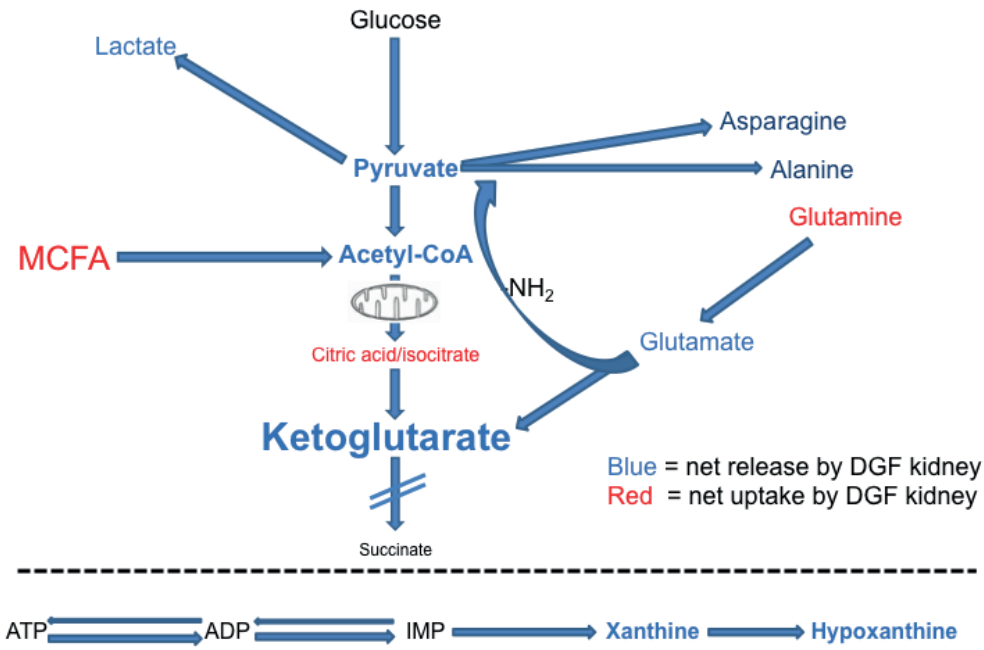

Supplemental Figure 2 summarizes the metabolic adaptation of +DGF grafts after reperfusion. The release of hypoxanthine, the end-product of ATP catabolism, as shown on the bottomline, indicates that ATP production is insufficient in +DGF grafts.
Medium chain fatty acids (MCFA) provide acetyl-CoA via beta-oxidation; as does pyruvate via normoxic glycolysis.
Due to defects in mitochondrial OXPHOS the Krebs cycle is spilled over and the Krebs cycle entry product acetyl-CoA is released.
The insufficient ATP production activates compensatory pathways producing Krebs cycle intermediates.For instance, ongoing glutaminolysis produces α-ketoglutarate.
Due to defects in the enzyme oxoglutarate dehydrogenase, α-ketoglutarate is not converted into succinate and it is released from +DGF grafts.
All in all, the only effective pathway of ATP production is the breakdown of pyruvate into lactate, asparagine and alanine via normoxic glycolysis.

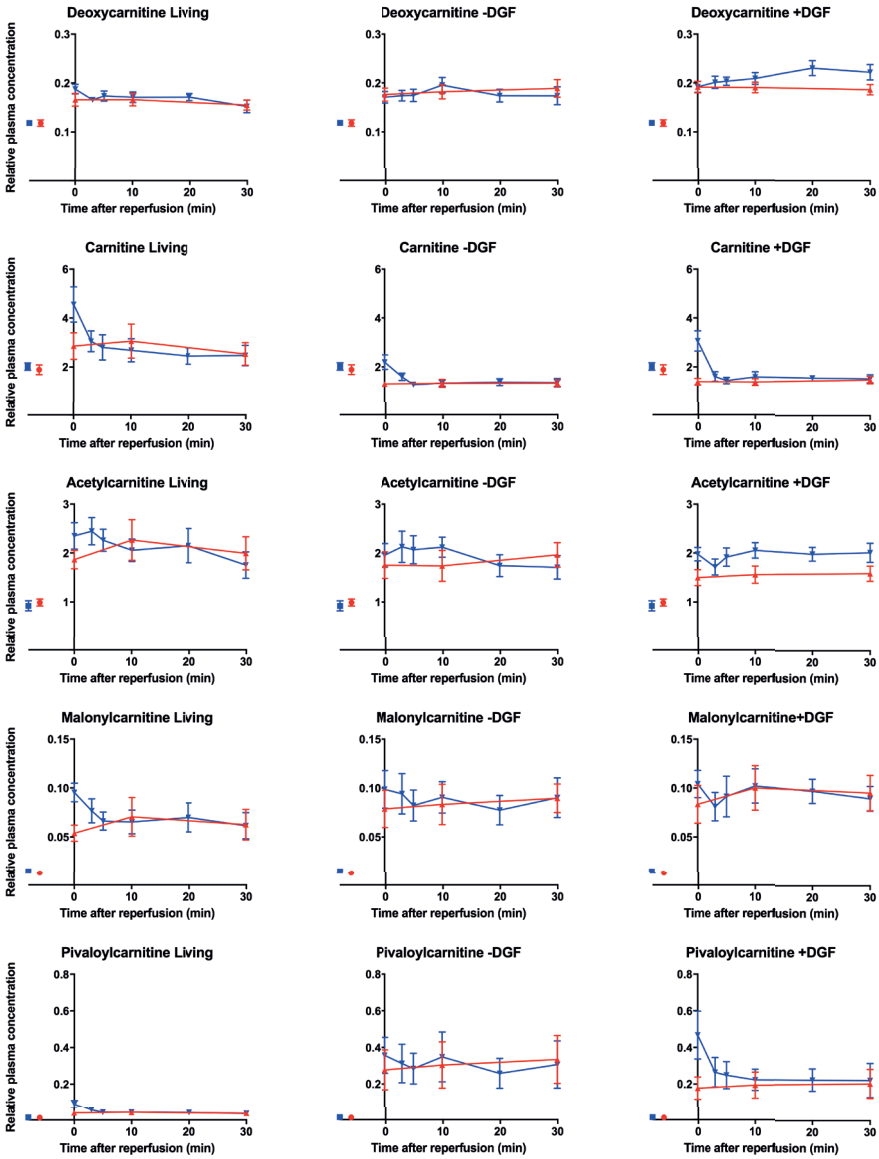
Deoxycarnitine Living
Deoxycarnitine -DGF
Deoxycarnitine +DGF
Carnitine Living
Carnitine -DGF
Carnitine +DGF
Acetylcarnitine Living
Acetylcarnitine -DGF
Acetylcarnitine +DGF
Malonylcarnitine Living
Malonylcarnitine -DGF
Malonylcarnitine+DGF
Pivaloylcarnitine Living
Pivaloylcarnitine -DGF
Pivaloylcarnitine +DGF
Relative plasma concentration
Time after reperfusion (min)
C2
C3
C4

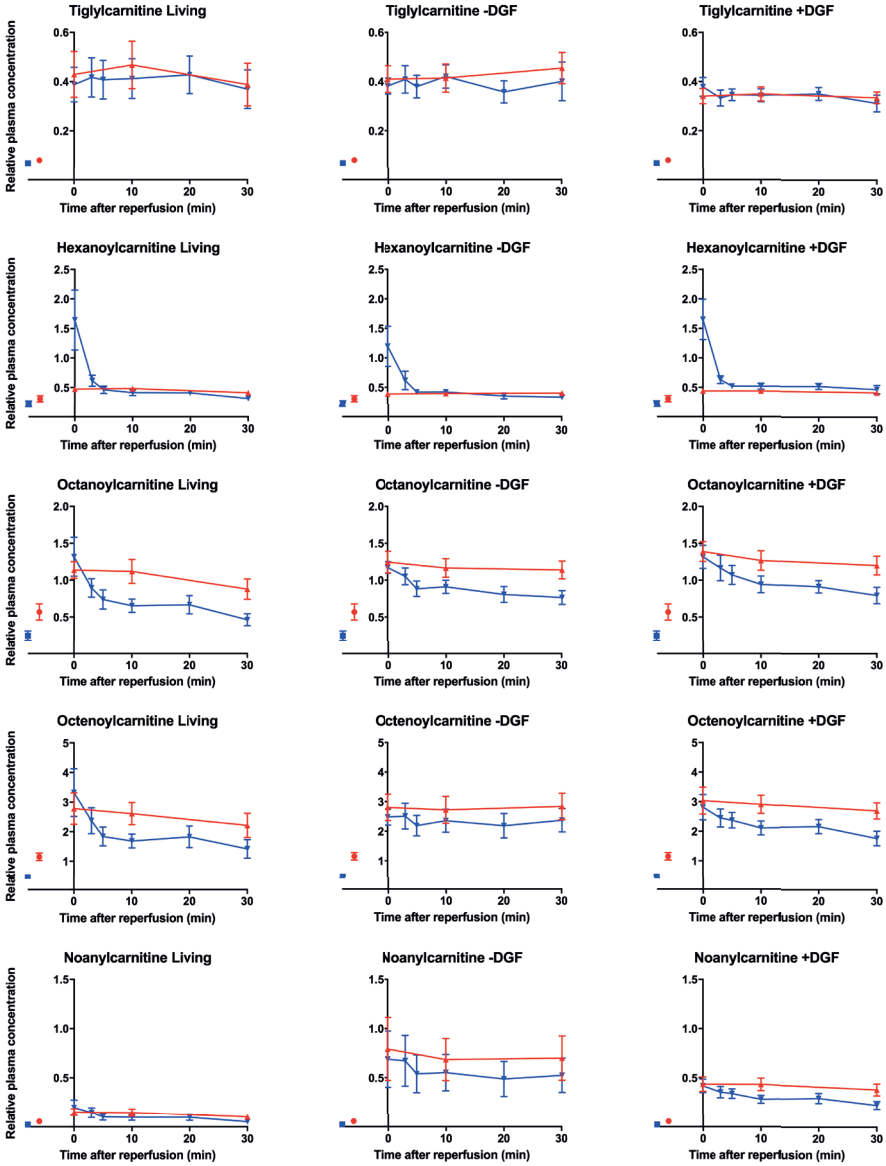
Tiglylcarnitine Living
Tiglylcarnitine -DGF
Tiglylcarnitine +DGF
C5
Hexanoylcarnitine Living
Hexanoylcarnitine -DGF
Hexanoylcarnitine +DGF
C6
Octanoylcarnitine Living
Octanoylcarnitine -DGF
Octanoylcarnitine +DGF
C7
Octenoylcarnitine Living
Octenoylcarnitine -DGF
Octenoylcarnitine +DGF
C8
Noanylcarnitine Living
Noanylcarnitine -DGF
Noanylcarnitine +DGF
C9
Relative plasma concentration
Time after reperfusion (min)

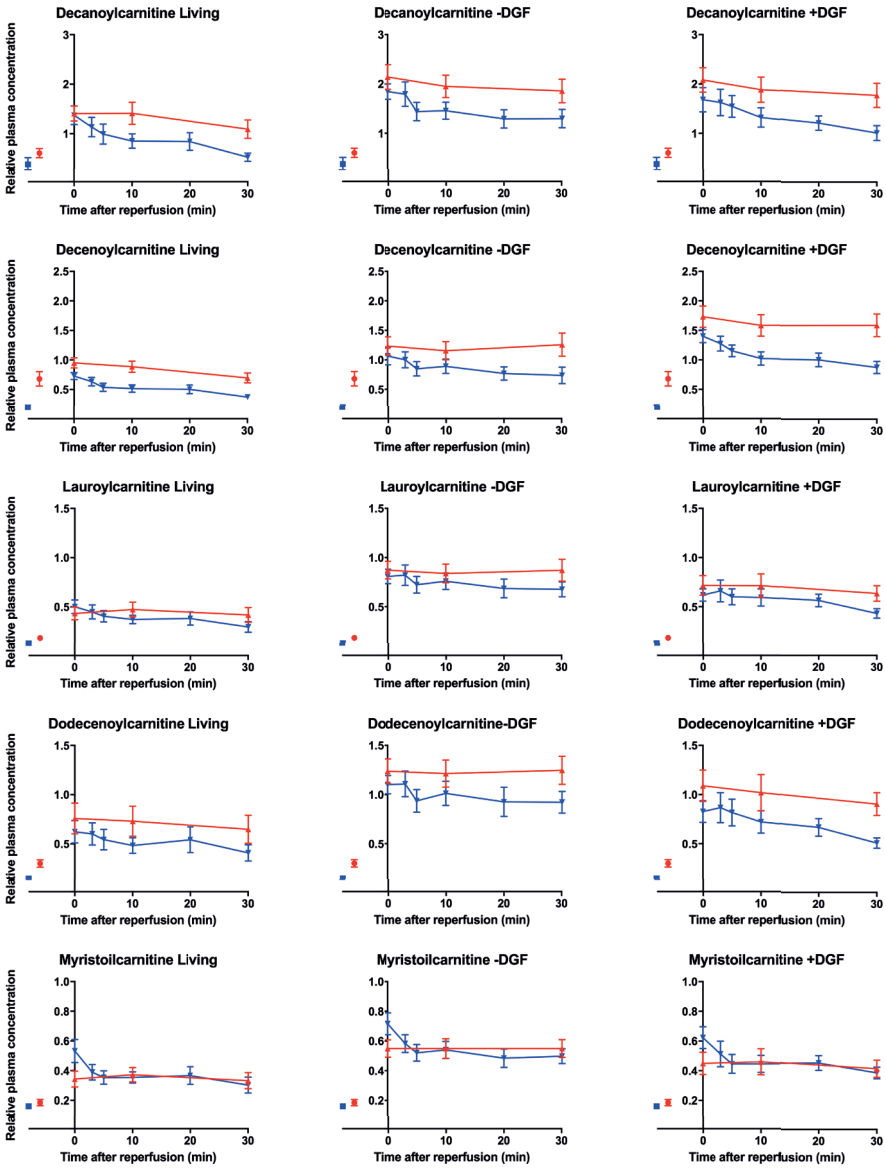
Decanoylcarnitine Living
Decanoylcarnitine -DGF
Decanoylcarnitine +DGF
C10
Decenoylcarnitine Living
Decenoylcarnitine -DGF
Decenoylcarnitine +DGF
C10
Lauroylcarnitine Living
Lauroylcarnitine -DGF
Lauroylcarnitine +DGF
C12
Dodecenoylcarnitine Living
Dodecenoylcarnitine-DGF
Dodecenoylcarnitine +DGF
C12
Myristoilcarnitine Living
Myristoilcarnitine -DGF
Myristoilcarnitine +DGF
C14
Relative plasma concentration
Time after reperfusion (min)

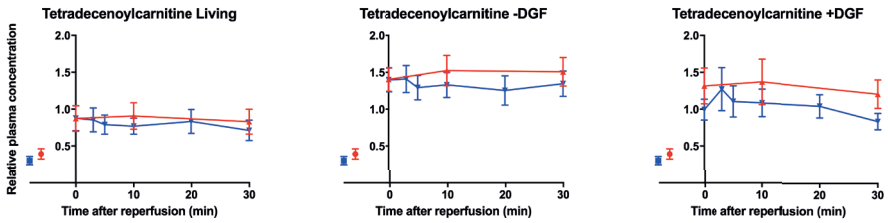

C14

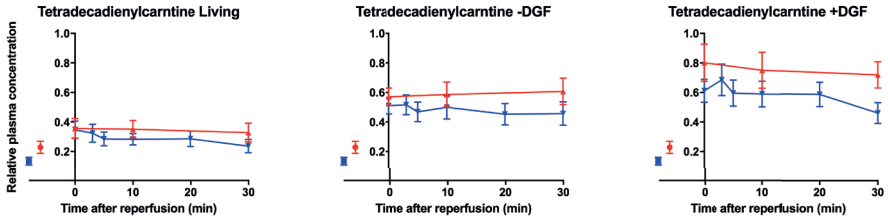

C14

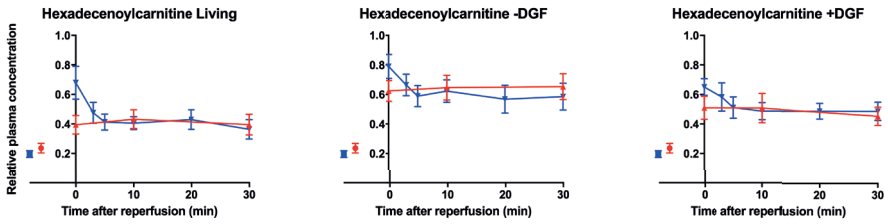

C16

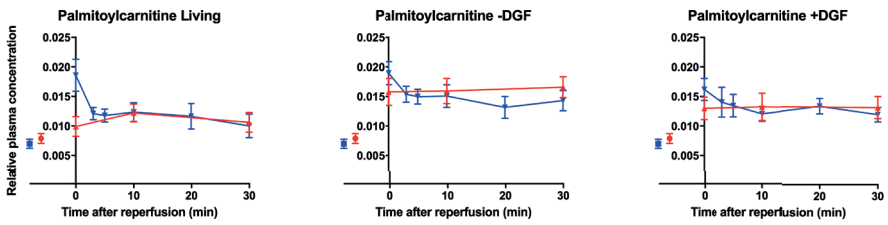

C16

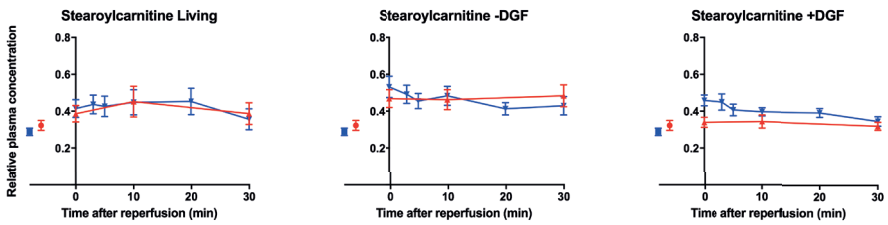

C18

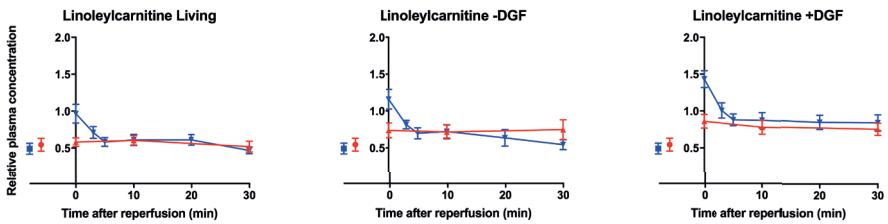

C18

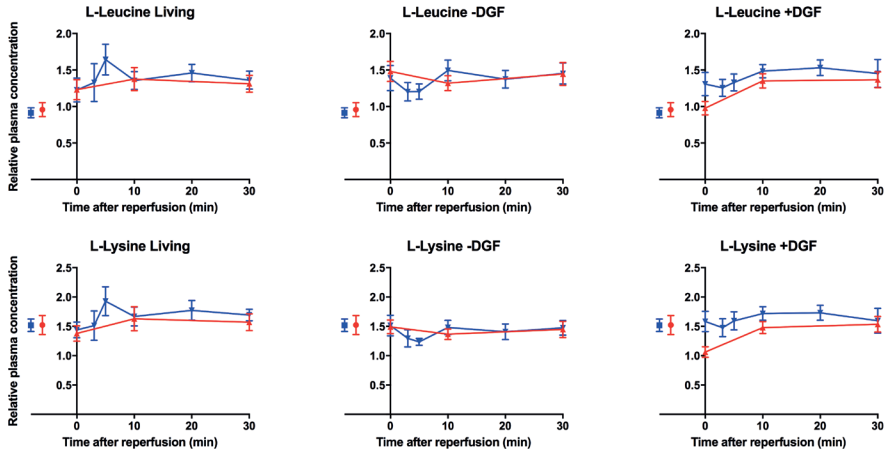
L-Leucine Living
L-Leucine -DGF
L-Leucine +DGF
L-Lysine Living
L-Lysine -DGF
L-Lysine +DGF
Relative plasma concentration
Time after reperfusion (min)
Ketogenic

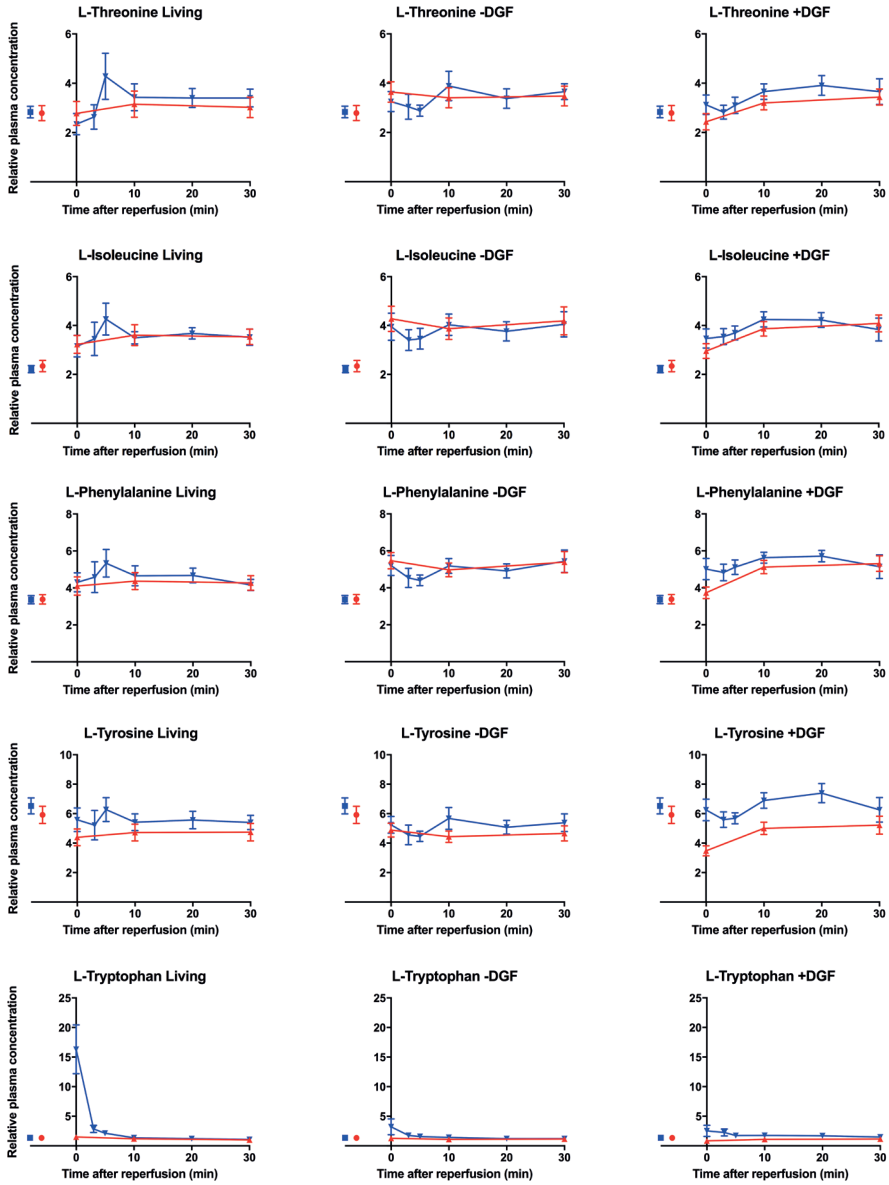

Ketogenic & glucogenic

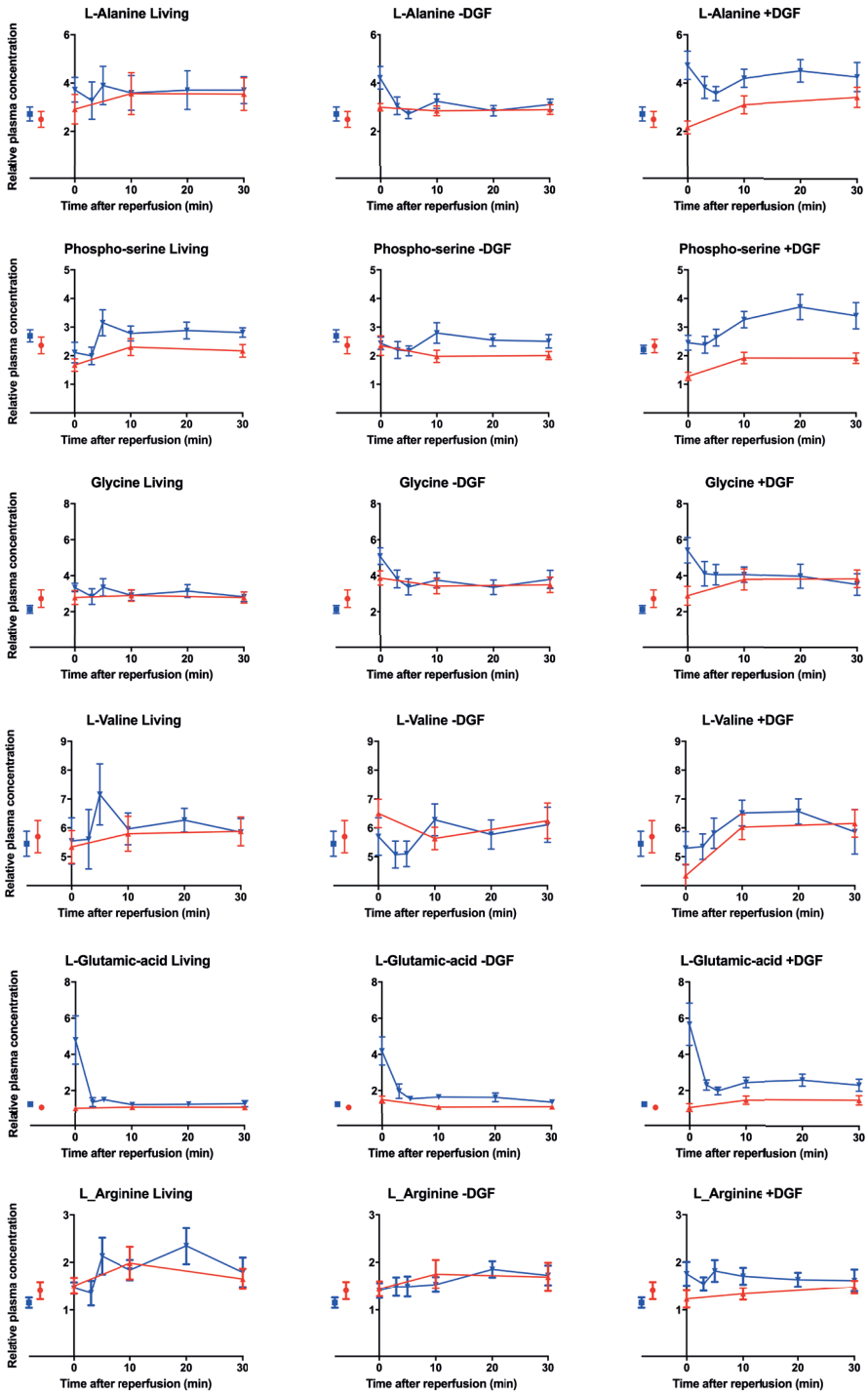
L-Alanine Living
L-Alanine -DGF
L-Alanine +DGF
Phospho-serine Living
Phospho-serine -DGF
Phospho-serine +DGF
Glycine Living
Glycine -DGF
Glycine +DGF
L-Valine Living
L-Valine -DGF
L-Valine +DGF
L-Glutamic-acid Living
L-Glutamic-acid -DGF
L-Glutamic-acid +DGF
L_Arginine Living
L_Arginine -DGF
L_Arginine +DGF
Relative plasma concentration
Time after reperfusion (min)

Glucogenic

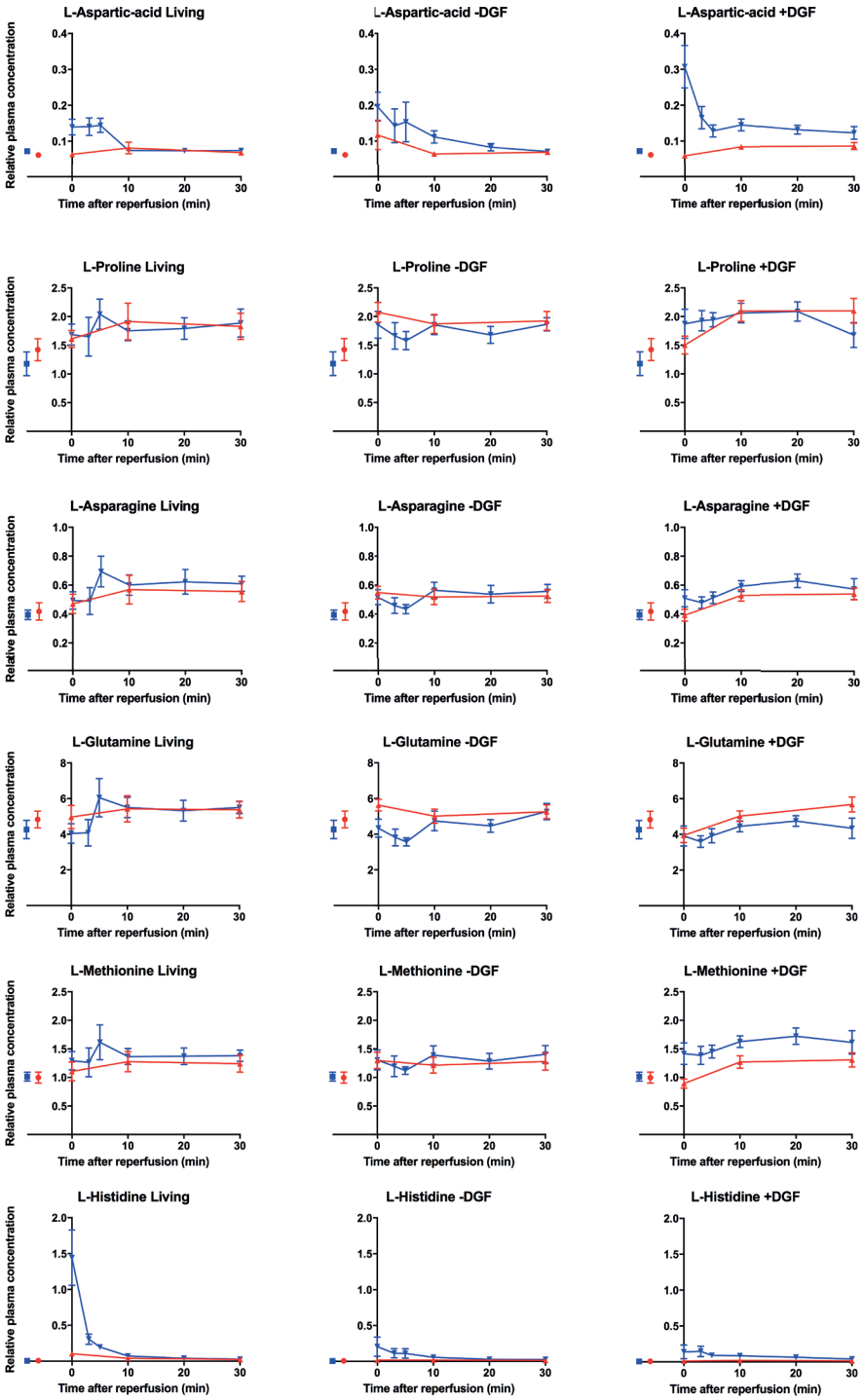

Glucogenic (cont.)

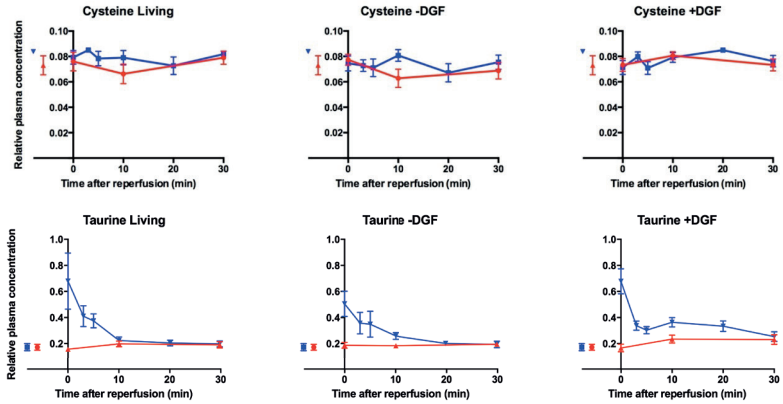
Cysteine Living
Cysteine -DGF
Cysteine +DGF
Taurine Living
Taurine -DGF
Taurine +DGF
Relative plasma concentration
Time after reperfusion (min)

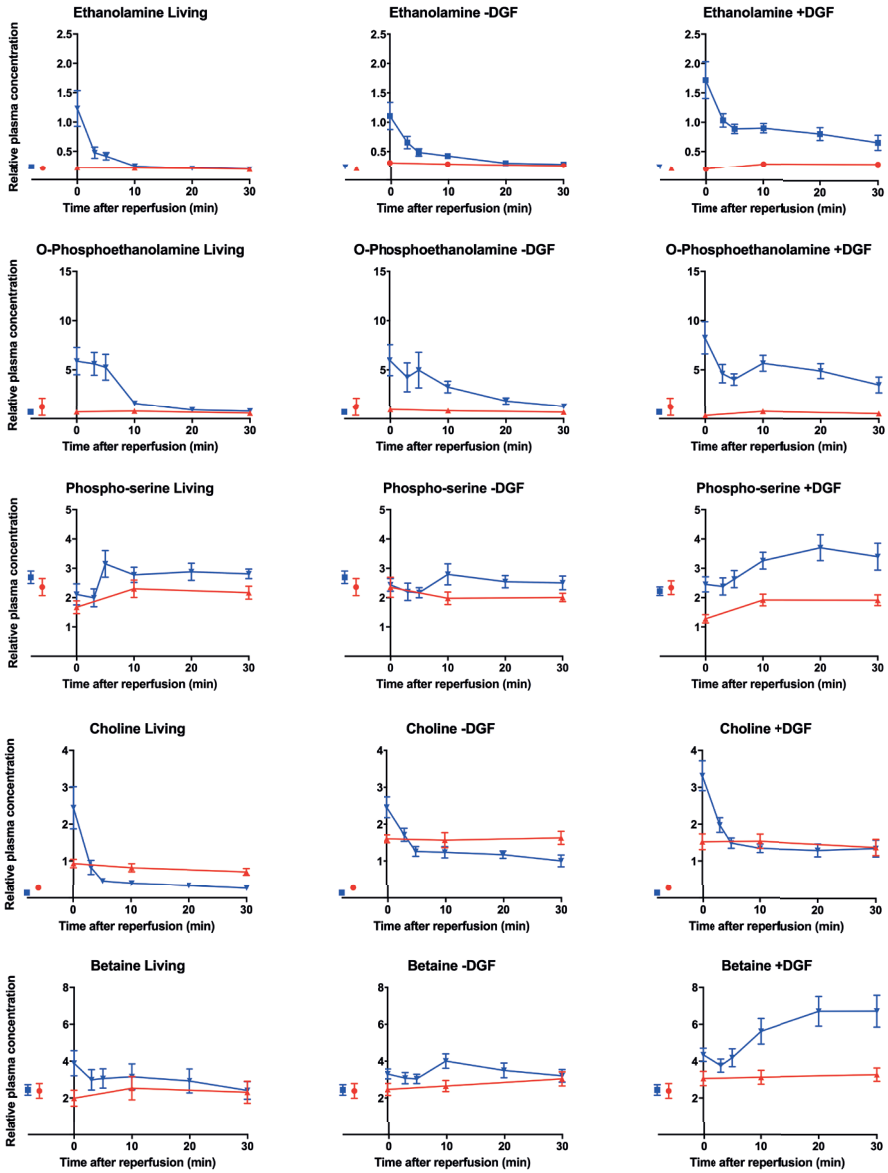

Phospholypolysis

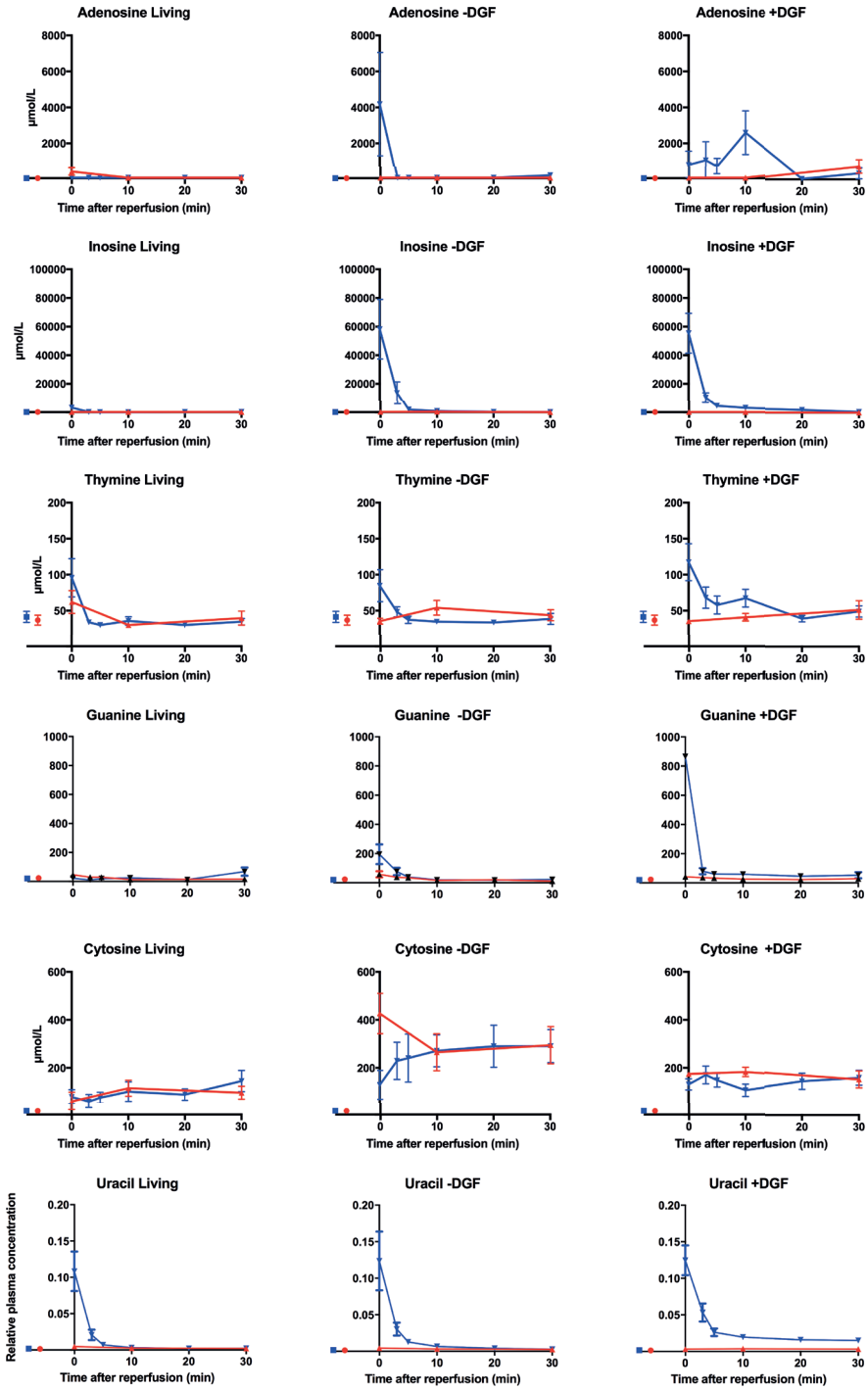

Nucleosides

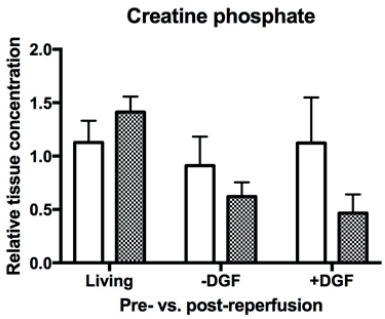
Creatine phosphate
Relative tissue concentration
2.0
1.5
1.0
0.5
0.0
Living
-DGF
+DGF
Pre- vs. post-reperfusion

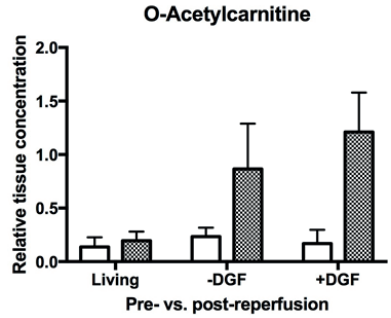
O-Acetylcarnitine
Relative tissue concentration
2.0
1.5
1.0
0.5
0.0
Living
-DGF
+DGF
Pre- vs. post-reperfusion

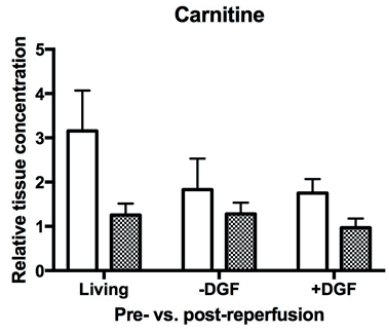
Carnitine
Relative tissue concentration
5
4
3
2
1
0
Living
-DGF
+DGF
Pre- vs. post-reperfusion

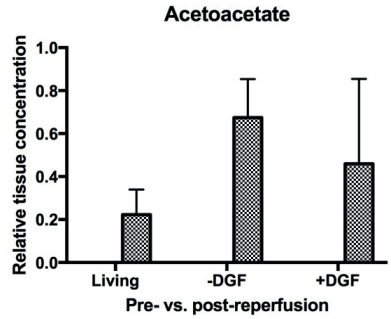
Acetoacetate
Relative tissue concentration
1.0
0.8
0.6
0.4
0.2
0.0
Living
-DGF
+DGF
Pre- vs. post-reperfusion

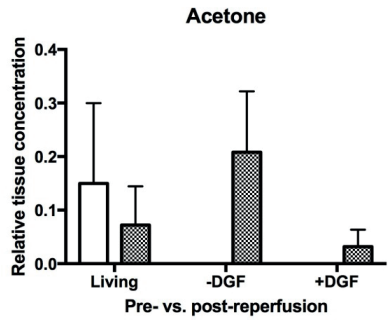
Acetone
Relative tissue concentration
0.4
0.3
0.2
0.1
0.0
Living
-DGF
+DGF
Pre- vs. post-reperfusion

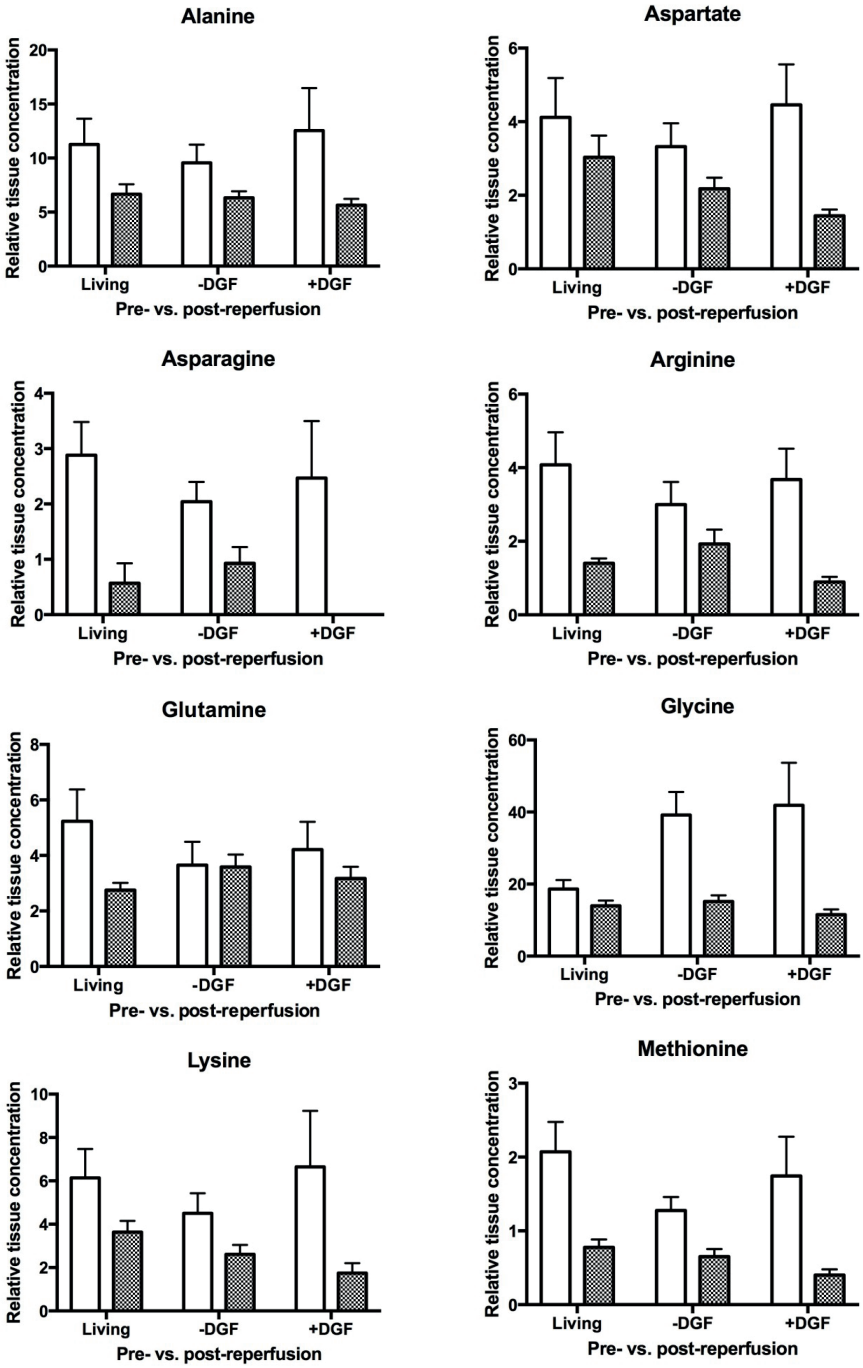
Alanine
Relative tissue concentration
0
5
10
15
20
Living
-DGF
+DGF
Pre- vs. post-reperfusion
Aspartate
Relative tissue concentration
0
2
4
6
Living
-DGF
+DGF
Pre- vs. post-reperfusion
Asparagine
Relative tissue concentration
0
1
2
3
4
Living
-DGF
+DGF
Pre- vs. post-reperfusion
Arginine
Relative tissue concentration
0
2
4
6
Living
-DGF
+DGF
Pre- vs. post-reperfusion
Glutamine
Relative tissue concentration
0
2
4
6
8
Living
-DGF
+DGF
Pre- vs. post-reperfusion
Glycine
Relative tissue concentration
0
20
40
60
Living
-DGF
+DGF
Pre- vs. post-reperfusion
Lysine
Relative tissue concentration
0
2
4
6
8
10
Living
-DGF
+DGF
Pre- vs. post-reperfusion
Methionine
Relative tissue concentration
0
1
2
3
Living
-DGF
+DGF
Pre- vs. post-reperfusion

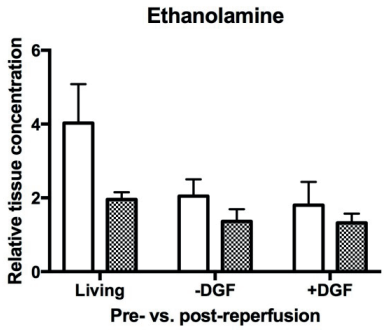
Ethanolamine
Relative tissue concentration
0
2
4
6
Living
-DGF
+DGF
Pre- vs. post-reperfusion

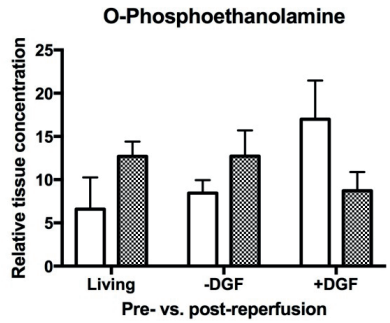
O-Phosphoethanolamine
Relative tissue concentration
0
5
10
15
20
25
Living
-DGF
+DGF
Pre- vs. post-reperfusion

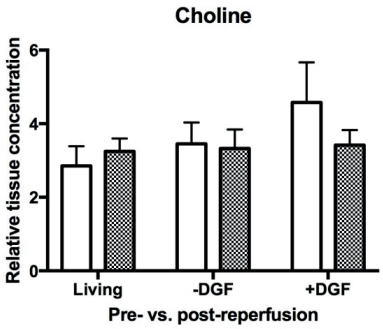
Choline
Relative tissue concentration
0
2
4
6
Living
-DGF
+DGF
Pre- vs. post-reperfusion

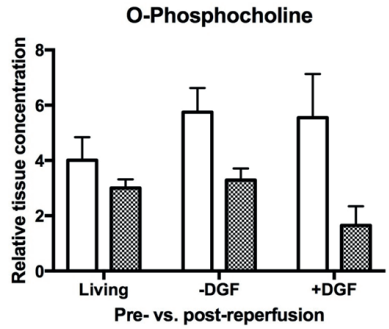
O-Phosphocholine
Relative tissue concentration
0
2
4
6
8
Living
-DGF
+DGF
Pre- vs. post-reperfusion

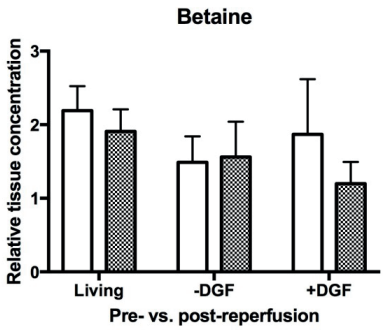
Betaine
Relative tissue concentration
0
1
2
3
Living
-DGF
+DGF
Pre- vs. post-reperfusion

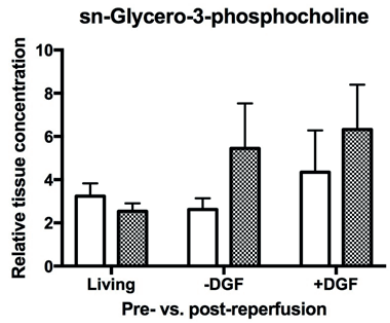
sn-Glycero-3-phosphocholine
Relative tissue concentration
0
2
4
6
8
10
Living
-DGF
+DGF
Pre- vs. post-reperfusion

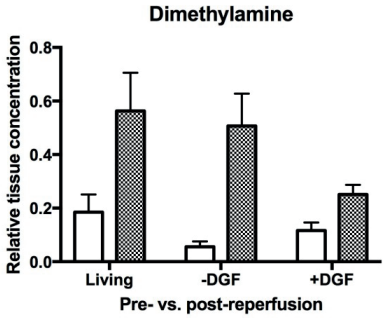
Dimethylamine
Relative tissue concentration
0.8
0.6
0.4
0.2
0.0
Living
-DGF
+DGF
Pre- vs. post-reperfusion

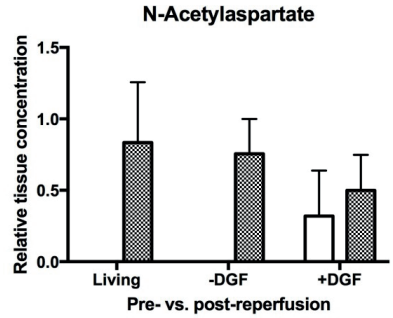
N-Acetylaspartate
Relative tissue concentration
1.5
1.0
0.5
0.0
Living
-DGF
+DGF
Pre- vs. post-reperfusion

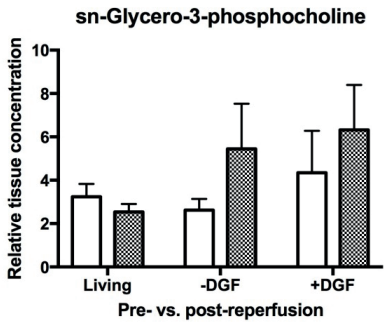
sn-Glycero-3-phosphocholine
Relative tissue concentration
10
8
6
4
2
0
Living
-DGF
+DGF
Pre- vs. post-reperfusion

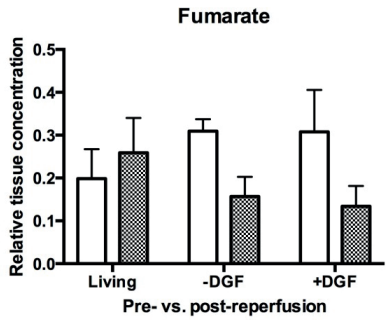
Fumarate
Relative tissue concentration
0.5
0.4
0.3
0.2
0.1
0.0
Living
-DGF
+DGF
Pre- vs. post-reperfusion

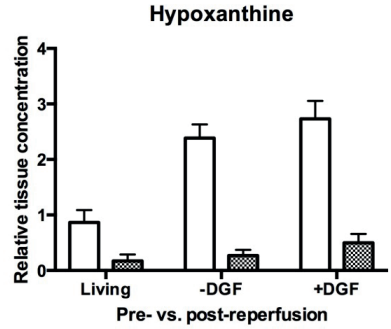
Hypoxanthine
Relative tissue concentration
4
3
2
1
0
Living
-DGF
+DGF
Pre- vs. post-reperfusion

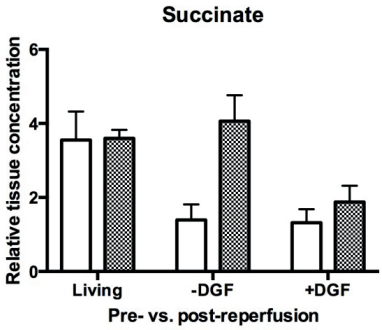
Succinate
Relative tissue concentration
6
4
2
0
Living
-DGF
+DGF
Pre- vs. post-reperfusion

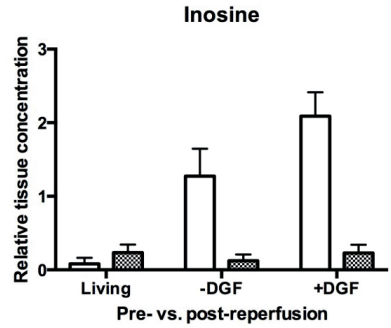
Inosine
Relative tissue concentration
3
2
1
0
Living
-DGF
+DGF
Pre- vs. post-reperfusion

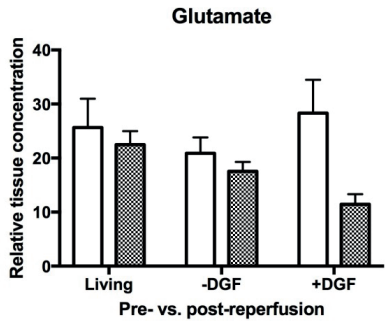
Glutamate
Relative tissue concentration
40
30
20
10
0
Living
-DGF
+DGF
Pre- vs. post-reperfusion

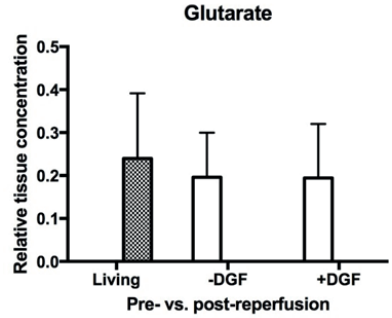
Glutarate
Relative tissue concentration
0.5
0.4
0.3
0.2
0.1
0.0
Living
-DGF
+DGF
Pre- vs. post-reperfusion

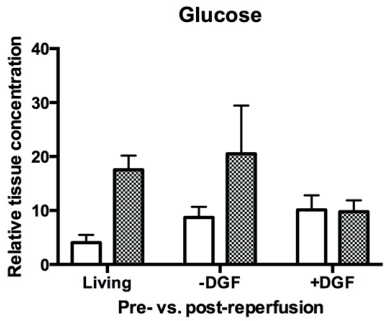
Glucose
Relative tissue concentration
40
30
20
10
0
Living
-DGF
+DGF
Pre- vs. post-reperfusion

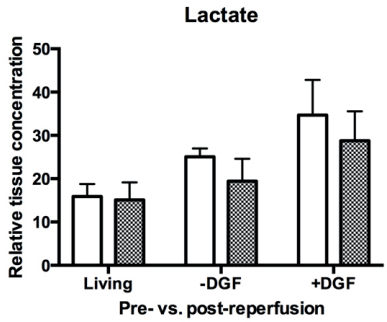
Lactate
Relative tissue concentration
50
40
30
20
10
0
Living
-DGF
+DGF
Pre- vs. post-reperfusion

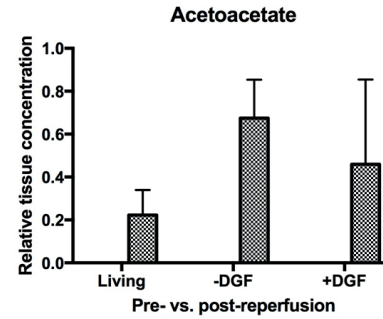
Acetoacetate
Relative tissue concentration
1.0
0.8
0.6
0.4
0.2
0.0
Living
-DGF
+DGF
Pre- vs. post-reperfusion

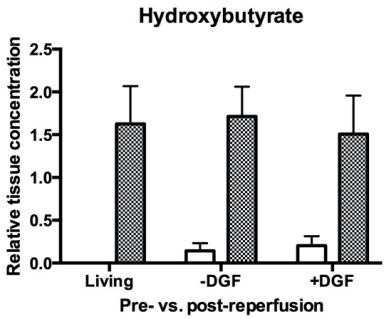
Hydroxybutyrate
Relative tissue concentration
2.5
2.0
1.5
1.0
0.5
0.0
Living
-DGF
+DGF
Pre- vs. post-reperfusion

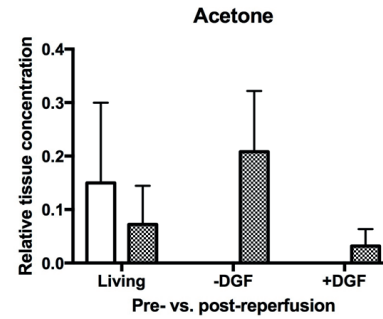
Acetone
Relative tissue concentration
0.4
0.3
0.2
0.1
0.0
Living
-DGF
+DGF
Pre- vs. post-reperfusion

SUPPLEMENTARY TABLES

Supplemental Table 1. Statistics metabolomics

Metabolite (pathway)	*Timepoint*	*Levels groups*	*P-value*
POWER OUTAGE			
Phosphocreatine	Post-reperfusion biopsy	+DGF: 0,39(0,19) mean(SEM) vs. control living: 1,41(0,35)	P=0,002
Hypoxanthine	Arteriovenous T=30	+DGF: arterial 3452,98(553,85) nmol/l mean(SEM) vs venous levels 17391,25(5042,63) nmol/l	P=0,007
Xanthine	Arteriovenous T=30	+DGF: arterial 2404,09(641,66) nmol/l mean(SEM) vs venous levels 4782,32(924,72) nmol/l	P=0,040
KREBS CYCLE DEFECT			
Acetylcarnitine	Post-reperfusion biopsy	controls 0,19(0,09) mean(SEM) vs. +DGF 1,45(0,34)	P=0,004
Acetylcarnitine	AV difference T=30	Living: 0.22(0.17) µmol/l mean(SEM) vs. +DGF: 0.45(0.16) µmol/l	P=0,016
Pyruvate	Area under the curve (venous vs. arterial curve) of To-T30 min	+DGF: 4,04(1,68) µmol/l mean(SEM)	P=0,022
Pyruvate	Area under the curve (venous vs. arterial curve) of To-T30 min	Living: 1,96(2,37)µmol/l mean(SEM)	P=0,41
Pyruvate	Area under the curve (venous vs. arterial curve) of To-T30 min	-DGF: 1,45(2,12) µmol/l mean(SEM)	P=0,49
a-Keto-glutarate	Arteriovenous T=30	+DGF: arterial 0,018(0,003) µmol/l mean(SEM) vs venous levels 0,037(0,007) µmol/l	P=0,008
Lactate	Arteriovenous T=30	+DGF: arterial 10,64(0,84) µmol/l mean(SEM) vs venous levels 16,34(1,40) µmol/l	P=0,001
Succinate	Pre-reperfusion biopsy vs. post-reperfusion biopsy	-DGF: pre 1,39(0,42) mean(SEM) vs. post 4,06(0,70)	P=0,007
Succinate	Post-reperfusion biopsies	Living vs. –DGF vs. +DGF. ANOVA	P=0,007
Succinic acid	Arteriovenous T=0	AV difference at T=0: 0,51(0.18) µmol/l mean(SEM) in living donor grafts vs. 0.21(0.07) µmol/l in +DGF grafts	P=0,095

Malic acid	Arteriovenous T=0	AV difference at T=0: 0.33(0.10) µmol/l mean(SEM) in living donor grafts vs. 0.18(0.06) µmol/l in +DGF grafts	P=0,182
Fumaric acid	Arteriovenous T=0	AV difference at T=0: 0,043(0.011) µmol/l mean(SEM) in living donor grafts vs. 0.023(0.006) µmol/l in +DGF grafts	P=0,114
ANAEROBIC GLYCOLYSIS			
Lactate	Arteriovenous T=30	+DGF: arterial 10,64(0,84) µmol/l mean(SEM) vs venous levels 16,34(1,40) µmol/l	P=0,001
Glucose	Post-reperfusion biopsies	Living: 17,54(2,64) mean(SEM) vs. +DGF 9,80(2,08)	P=0,044
Pyruvate	Area under the curve (venous vs. arterial curve) of To-T30 min	+DGF: 4,04(1,68) µmol/l mean(SEM)	P=0,022
GLUTAMINOLYSIS			
Glutamic acid	Arteriovenous T=30	+DGF: arterial 0,97(0,17) µmol/l mean(SEM) vs venous levels 1,82(0,25) µmol/l;	P=0,006
α-Ketoglutarate	Arteriovenous T=30	+DGF: arterial 0,018(0,003) µmol/l mean(SEM) vs venous levels 0,037(0,007) µmol/l	P=0,008
Alanine	Area under the curve (venous minus arterial curve) of To-T30 min	Living 7,09(8,85) mean(SEM) vs. – DGF 6,74(7,93) vs. +DGF 38,59(6,32); ANOVA	P=0,006
Aspartic acid	Arteriovenous T=30	+DGF: arterial 0,050(0,004) µmol/l mean(SEM) vs venous levels 0,106(0,021) µmol/l	P=0,005
Pyruvic acid	Area under the curve (venous minus arterial curve) of To-T30 min	+DGF: 4,04(1,68) µmol/l mean(SEM)	P=0,022
Glutamate	Pre-reperfusion biopsy vs. post-reperfusion biopsy	+DGF: pre 28,20(6,17) mean(SEM) vs. post 9,62(0,59)	P=0,017
Asparagine	Pre-reperfusion biopsy vs. post-reperfusion biopsy	Living: pre 2,88(0,60) mean(SEM) vs. post 0,57(0,36)	P=0,008
Asparagine	Pre-reperfusion biopsy vs. post-reperfusion biopsy	-DGF: pre 2,04(0,36) mean(SEM) vs. post 1,08(0,29)	P=0,067

Asparagine	Pre-reperfusion biopsy vs. post-reperfusion biopsy	+DGF: pre 2,47(1,03) mean(SEM) vs. post 0,00(0,00)	P=0,026
Alanine	Pre-reperfusion biopsy vs. post-reperfusion biopsy	Living: pre 11,26(2,39) mean(SEM) vs. post 6,65(0,95)	P=0,102
Alanine	Pre-reperfusion biopsy vs. post-reperfusion biopsy	-DGF: pre 9,56(1,68) mean(SEM) vs. post 6,33(0,59)	P=0,094
Alanine	Pre-reperfusion biopsy vs. post-reperfusion biopsy	+DGF: pre 12,54(3,94) mean(SEM) vs. post 5,65(1,44)	P=0,089
BETA-OXIDATION			
Valerylcarnitine	Arteriovenous T=30	+DGF: arterial 0,019(0,002) µmol/l mean(SEM) vs venous levels 0,079(0,023) µmol/l	P=0,006
Methylbutyroylcarnitine	AV difference T=30	Living: -0.13(0.06) µmol/l mean(SEM) vs. +DGF: 0.21(0.1) µmol/l	P=0,006
Linoleylcarnitine	AV difference T=30	Living: -0.04(0.06) µmol/l mean(SEM) vs. +DGF: 0.12(0.06) µmol/l	P=0,022
3-Hydroxybutyrate	Pre-reperfusion biopsy vs. post-reperfusion biopsy	+DGF: pre 0,20(0,11) mean(SEM) vs. post 1,51(0,45)	P=0,031
O-acetylcarnitine	Post-reperfusion biopsies	Living: 0,19(0,09) mean(SEM) vs. +DGF 1,45(0,34)	P=0,004
PHOSPHOLIPOLYSIS			
Phospho-serine	Arteriovenous T=30	+DGF: arterial 1,91(0,19) µmol/l mean(SEM) vs venous levels 3,40(0,46) µmol/l	P=0,003
Phospho-ethanolamine	Arteriovenous T=30	+DGF: arterial 0,53(0,06) µmol/l mean(SEM) vs venous levels 3,42(0,82) µmol/l	P=0,001
O-phosphoethanolamine	Pre-reperfusion biopsy vs. post-reperfusion biopsy	+DGF: pre 17,0(4,48) mean(SEM) vs. post 6,59(0,64)	P=0,050
Ethanolamine	Arteriovenous T=30	+DGF: arterial 0,27(0,02) µmol/l mean(SEM) vs venous levels 0,65(0,13) µmol/l	P=0,004
O-phosphocholine	Pre-reperfusion biopsy vs. post-reperfusion biopsy	+DGF: pre 5,55(1,58) mean(SEM) vs. post 0,98(0,19)	P=0,021

Betaine	Arteriovenous T=30	+DGF: arterial 3,25(0,36) µmol/l mean(SEM) vs venous levels 6,70(0,87) µmol/l	P=0,0004
Methionine	Area under the curve (venous minus arterial curve) of To-T30 min	Living: 5,92(3,49) mean(SEM)	P=0,100
Methionine	Area under the curve (venous minus arterial curve) of To-T30 min	–DGF: 1,15(3,12) mean(SEM)	P=0,370
Methionine	Area under the curve (venous minus arterial curve) of To-T30 min	+DGF: 13,50(2,49) mean(SEM	P=0,000006
Isovaleryl-carnitine	Arteriovenous T=30	+DGF: arterial 0,26(0,02) µmol/l mean(SEM) vs venous levels 0,55(0,09) µmol/l	P=0,001
Choline	Arteriovenous T=30	Living: arterial 0,71(0,09) µmol/l mean(SEM) vs venous levels 0,27(0,08) µmol/l	P=0,001
Choline	Arteriovenous T=30	+DGF: 1,63(0,18) µmol/l mean(SEM) vs venous levels 1,01(0,48) µmol/l;	P=0,018
Methionine	Pre-reperfusion biopsy vs. post-reperfusion biopsy	Living pre 2,07(0,40) mean(SEM) vs. post 0,78(0,1)	P=0,011
Methionine	Pre-reperfusion biopsy vs. post-reperfusion biopsy	-DGF pre 1,28(0,18) mean(SEM) vs. post 0,65(0,10)	P=0,012
Methionine	Pre-reperfusion biopsy vs. post-reperfusion biopsy	+DGF pre 1,74(0,53) mean(SEM) vs. post 0,40(0,08)	
	P=0,023		
Leucine	Area under the curve (venous minus arterial curve) of To-T30 min	Living = 3,94(3,19) mean(SEM)	P=0,227
Leucine	Area under the curve (venous minus arterial curve) of To-T30 min	–DGF -0,72(2,85) mean(SEM)	P=0,802
Leucine	Area under the curve (venous minus arterial curve) of To-T30 min	+DGF 5,74(2,28) mean(SEM)	P=0,017
Lysine	Area under the curve (venous minus arterial curve) of To-T30 min	Living = 5,56(4,03) mean(SEM)	P=0,178

Lysine	Area under the curve (venous minus arterial curve) of To-T30 min	–DGF -0,85(3,60) mean(SEM)	P=0,815
Lysine	Area under the curve (venous minus arterial curve) of To-T30 min	+DGF 8,42(2,87) mean(SEM)	P=0,006
Tyrosine	Area under the curve (venous minus arterial curve) of To-T30 min	Living = 34,09(14,12) mean(SEM)	P=0,022
Tyrosine	Area under the curve (venous minus arterial curve) of To-T30 min	–DGF 18,08 (12,61) mean(SEM)	P=0,162
Tyrosine	Area under the curve (venous minus arterial curve) of To-T30 min	+DGF 66,02(10,07) mean(SEM)	P=2,399 3E-7
CELL DAMAGE			
Uracil	Arteriovenous T=30	+DGF: arterial 0,003(0,0004) µmol/l mean(SEM) vs venous levels 0,015(0,0032) µmol/l	P=0,002

Supplementary Methods

METABOLITE ANALYSIS METHODS

General information

Samples were stored at -80°C until used further analysis. All samples were randomized and run in 5 batches which included a calibration line, QC samples and blanks. QC samples were analyzed every 10 samples (or every 15 samples in the oxidative stress platform). The acquired data were evaluated using MassHunter software (Agilent). An in-house written tool is applied using the QC samples to compensate for shifts in the sensitivity of the mass spectrometer throughout the batches.[21] Both internal standard correction and QC correction were applied to the data set before reporting results. All metabolites comply with the acceptance criteria of RSDQC <30%.

1. BIOGENIC AMINE PROFILING

The amine platform covers amino acids and biogenic amines employing an Accq-tag derivatization strategy adapted from the protocol supplied by Waters. 5 µL of each plasma sample was spiked with an internal standard solution, thiol amines are released from proteins and converted to reduced using TCEP. Then proteins are precipitated by the addition of methanol. The supernatant was transferred to a new eppendorf tube and taken to dryness in a speedvac. The residue was reconstituted in borate buffer (pH 8.5) with AQC reagent. After reaction, the vials were transferred to an autosampler tray and cooled to 10°C until the injection. 1.0 µL of the reaction mixture was injected into the UPLC-MS/MS system.

An Agilent 1290 Infinity UHPLC system with autosampler (Agilent, The Netherlands) was coupled online with a 6490 Triple quadrupole mass spectrometer (Agilent) operated using MassHunter data acquisition software (B.04.01; Agilent). The samples were analyzed by UPLC-MS/MS using an Accq-Tag Ultra column (Waters). The Triple quadrupole MS was used in the positive-ion electrospray mode and all analytes were monitored in dynamic Multiple Reaction Monitoring (dMRM) using nominal mass resolution.[22]

2. ORGANIC ACID PROFILING

This profiling platform, performed with GC-MS technology, covers 28 organic acids. Sample preparation was done by doing first protein precipitation of 50 uL of plasma with a crash solvent (MeOH/H2O) with ISTD added. After centrifugation and transferring the supernatant, the solvent was evaporated to complete dryness on the speedvac. Then, two-step derivatisation procedures with oximation using methoxyamine hydrochloride (MeOX, 15mg/mL in pyridine) as first reaction

and silylation using N-Methyl-N-(trimethylsilyl) trifluoroacetamide (MSTFA) as second reaction were carried out. After this final step the samples were transferred to the auto sampler vials and 1 µL was injected on GC-MS20.

The metabolites were measured by gas chromatography on an Agilent Technologies 7890A equipped with an Agilent Technologies mass selective detector (MSD 5975C) and MultiPurpose Sampler (MPS, MXY016-02A, GERSTEL). Chromatographic separations were performed on a HP-5MS UI (5% Phenyl Methyl Silox), 30 m × 0.25 m ID column with a film thickness of 25 m, using helium as the carrier gas at a flow rate of 1,7 mL/min. A single-quadrupole mass spectrometer with electron impact ionization (EI, 70 eV) was used. The mass spectrometer was operated in SCAN mode mass range 50-500.[23]

3. ACYLCARNITINE PROFILING

The acylcarnitine platform covers acylcarnitines as well as Trimethylamine-N-oxide, Choline, Betaine, Deoxycarnitine and Carnitine. 10 µL of each sample was spiked with an internal standard solution and proteins were precipitated by the addition of MeOH. The supernatant was transferred to an autosampler vial. The vials were transferred to an autosampler tray and cooled to 4 until the injection. 1.0 µL of the reaction mixture was injected into the triple quadrupole mass spectrometer.

Chromatographic separation was achieved by UPLC (Agilent 1100, San Jose, CA, USA) on an Accq- Tag Ultra column (Waters) with a flow of 0.7 mL/min over a 11 min gradient. The UPLC was coupled to electrospray ionization on a triple quadrupole mass spectrometer (Agilent 6460, San Jose, CA, USA). Analytes were detected in the positive ion mode and monitored in Multiple Reaction Monitoring (MRM) using nominal mass resolution.

4.PURINES AND PYRIMIDINES

Purines and pyrimidines were identified by using an in-house developed UPLC-MS/MS method. Briefly 30 µl plasma was mixed with 30 µl of a solution containing stable isotope labelled internal standards. Samples were deproteinized with 500 µl acetonitrile. After centrifugation (10 min, 12000 rpm, 4°C) the supernatant was evaporated under nitrogen and reconstituted in 500 µl 50 mM ammoniumformate buffer (pH=4.00).

Purine and pyrimidine metabolites were separated using a Waters Acquity UPLC system (Waters, Etten-Leur, The Netherlands) equipped with an Acquity HSS T3 (2.1 * 100 mm, df 1.8 µm). Separation of the compounds of interest was achieved by a 0.01 M ammonium formate (pH=4.00) / acetonitrile gradient. Compounds were quantified using a Waters XEVO TQS tandem mass spectrometer (Waters, Etten-

Leur, The Netherlands), both in negative or positive electrospray ionization using specific MRM transitions.

5. MAGIC ANGLE SPINNING HIGH-RESOLUTION NMR SPECTROSCOPY (MAS HR-NMR)

Metabolic profiling of the tissue biopsies was performed by MAS HR-NMR spectrometry on a 14.1 T Bruker Avance III spectrometer. All measurements were performed at the MR Core Facility, Norwegian University of Science and Technology (NTNU). MR core facility is funded by the Faculty of Medicine at NTNU and Central Norway Regional Health Authority. Samples were prepared on ice and fitted in a leak-proof insert (30 µL, Bruker: Kel-F, Bruker, Delft, The Netherlands) used in a zirconium MAS rotor (4 mm). The insert was filled with 3 µL cold (4°C) phosphate-buffered saline in D_2O containing 4.5 mM TSP-D_4 and 25 mM sodium formate ($CHNaO_2$) as internal standards. During NMR measurements the temperature was set to 4°C and the rotor spinning rate to 5 kHz. Per sample, a set of 3 NMR experiments were acquired including the 1D 1H NOESY, the 1D 1H CPMG and the 2D 1H J-resolved, with adjusted parameters as described previously.[24] An additional set of 2D NMR spectra for a subset of samples as well as the Bbio Refcode and ChenomX NMR suite 8.1 databases were used for identification of metabolites, while the latter was used for the quantification. In total, 41 compounds were quantified and their relative concentrations were normalized to tissue weight.

REFERENCES

1. Schroppel B, Legendre C: Delayed kidney graft function: from mechanism to translation. Kidney Int 2014; 86: 251-8
2. Mallon DH, Summers DM, Bradley JA, Pettigrew GJ: De ning delayed graft function after renal transplantation: simplest is best. Transplantation 2013; 96: 885-9
3. Yarlagadda SG, Coca SG, Formica RN, Jr., Poggio ED, Parikh CR: Association between delayed graft function and allograft and patient survival: a systematic review and meta-analysis. Nephrol Dial Transplant 2009; 24: 1039-47
4. Cavaille-Coll M, Bala S, Velidedeoglu E, Hernandez A, Archdeacon P, Gonzalez G, Neuland C, Meyer J, Albrecht R: Summary of FDA workshop on ischemia reperfusion injury in kidney transplantation. Am J Transplant 2013; 13: 1134-48
5. de Vries DK, Kortekaas KA, Tsikas D, Wijermars LG, van Noorden CJ, Suchy MT, Cobbaert CM, Klautz RJ, Schaapherder AF, Lindeman JH: Oxidative damage in clinical ischemia/reperfusion injury: a reappraisal. Antioxid Redox Signal 2013; 19: 535-45
6. de Vries DK, Lindeman JH, Ringers J, Reinders ME, Rabelink TJ, Schaapherder AF: Donor brain death predisposes human kidney grafts to a proin ammatory reaction after transplantation. Am J Transplant 2011; 11: 1064-70
7. de Vries DK, Lindeman JH, Tsikas D, de Heer E, Roos A, de Fijter JW, Baranski AG, van Pelt J, Schaapherder AF: Early renal ischemia-reperfusion injury in humans is dominated by IL-6 release from the allograft. Am J Transplant 2009; 9: 1574-84
8. de Vries DK, van der Pol P, van Anken GE, van Gijlswijk DJ, Damman J, Lindeman JH, Reinders ME, Schaapherder AF, Kooten C: Acute but transient release of terminal complement complex after reperfusion in clinical kidney transplantation. Transplantation 2013; 95: 816-20
9. Kortekaas KA, de Vries DK, Reinders ME, Lievers E, Ringers J, Lindeman JH, Schaapherder AF: Interleukin-9 release from human kidney grafts and its potential protective role in renal ischemia/reperfusion injury. In amm Res 2013; 62: 53-9
10. Wijermars LG, Schaapherder AF, de Vries DK, Verschuren L, Wust RC, Kostidis S, Mayboroda OA, Prins F, Ringers J, Bierau J, Bakker JA, Kooistra T, Lindeman JH: Defective postreperfusion metabolic recovery directly associates with incident delayed graft function. Kidney Int 2016; 90: 181-91
11. Chouchani ET, Pell VR, Gaude E, Aksentijevic D, Sundier SY, Robb EL, Logan A, Nadtochiy SM, Ord EN, Smith AC, Eyassu F, Shirley R, Hu CH, Dare AJ, James AM, Rogatti S, Hartley RC, Eaton S, Costa AS, Brookes PS, Davidson SM, Duchen MR, Saeb-Parsy K, Shattock MJ, Robinson AJ, Work LM, Frezza C, Krieg T, Murphy MP: Ischaemic accumulation of succinate controls reperfusion injury through mitochondrial ROS. Nature 2014; 515: 431-5
12. Ivanisevic J, Elias D, Deguchi H, Averell PM, Kurczy M, Johnson CH, Tautenhahn R, Zhu Z, Watrous J, Jain M, Grif n J, Patti GJ, Siuzdak G: Arteriovenous Blood Metabolomics: A Readout of Intra-Tissue Metabostasis. Sci Rep 2015; 5: 12757
13. Stoica SC: High-energy phosphates and the human donor heart. J Heart Lung Transplant 2004; 23: S244-6
14. Zuk A, Bonventre JV: Acute Kidney Injury. Annu Rev Med 2016; 67: 293-307
15. Burwell LS, Nadtochiy SM, Brookes PS: Cardioprotection by metabolic shut-down and gradual wake-up. J Mol Cell Cardiol 2009; 46: 804-10
16. Huber R, Spiegel T, Buchner M, Riepe MW: Graded reoxygenation with chemical inhibition of oxidative phosphorylation improves posthypoxic recovery in murine hippocampal slices. J Neurosci Res 2004; 75: 441-9

17. Szoleczky P, Modis K, Nagy N, Dori Toth Z, DeWitt D, Szabo C, Gero D: Identification of agents that reduce renal hypoxia-reoxygenation injury using cell-based screening: purine nucleosides are alternative energy sources in LLC-PK1 cells during hypoxia. Arch Biochem Biophys 2012; 517: 53-70
18. Shen H, Chen GJ, Harvey BK, Bickford PC, Wang Y: Inosine reduces ischemic brain injury in rats. Stroke 2005; 36: 654-9
19. Szabo G, Stumpf N, Radovits T, Sonnenberg K, Gero D, Hagl S, Szabo C, Bahrle S: Effects of inosine on reperfusion injury after heart transplantation. Eur J Cardiothorac Surg 2006; 30: 96-102
20. Hu Cea: RPLC-Ion-Trap-FTMS Method for Lipid Profiling of Plasma: Method Validation and Application to p53 Mutant Mouse Model. J. Proteome Res., ; 7: 4982–4991
21. Van der Kloet FM, Bobeldijk I, Verheij ER, Jellema RH. Analytical error reduction using single point calibration for accurate and precise metabolomic phenotyping. J. Proteome Res 2009; 8: 5132–5141
22. Noga MJ, Dane A, Shi S, Attali A, van Aken H, Suidgeest E, et al. Metabolomics of cerebrospinal fluid reveals changes in the central nervous system metabolism in a rat model of multiple sclerosis. Metabolomics 2012; 8: 253-263
23. Koek MM, van der Kloet FM, Kleemann R, Kooistra T, Verheij ER, Hankemeier T. Semi-automated non-target processing in GC × GC–MS metabolomics analysis: applicability for biomedical studies. Metabolomics 2011; 7: 1-14
24. Beckonert O, Keun HC, Ebbels TMD, Bundy J, Holmes E, Lindon JC, et al. Metabolic profiling, metabolomic and metabonomic procedures for NMR spectroscopy of urine, plasma, serum and tissue extracts. Nat Protoc 2007; 2: 2692–2703